© 2015 IJSRSET | Volume 1 | Issue 2 | Print ISSN : 2395-1990 | Online ISSN : 2394-4099
Themed Section: Engineering and Technology

Recent developments in T-Trefftz and F-Trefftz Finite Element Methods

Yi Xiao
Research School of Engineering, Australian National University, Acton, ACT 2601, Australia

ABSTRACT

This paper presents an overview of both T-Trefftz and F-Trefftz finite element methods (FEM) and its application in various engineering problems. Recent developments on the T-Trefftz finite element formulation of nonlinear problems of minimal surface, F-Trefftz methods for composite, skin tissue, and functionally graded materials are described. Formulations for all cases are derived by means of a modified variational functional and T-complete solutions or fundamental solutions. Generation of elemental stiffness equations from the modified variational principle is also discussed. Finally, a brief summary of the approach is provided and future trends in this field are identified.

Keywords: Finite Element Method, Trefftz Method, Fundamental Solution, Variational functional

I. INTRODUCTION

During the past decades, research into the development of efficient finite elements has mostly concentrated on the following four distinct types [1-7]. The first is the so-called conventional FEM. It is based on a suitable polynomial interpolation function which has already been used to analyse most physical problems. With this method, the solution domain is divided into a number of cells or elements, and material properties are defined at element level[1, 5]. The second is the natural-mode FEM initiated by Argyris et al [2, 8]. In contrast, the natural FEM presents a significant alternative to conventional FEM with ramifications on all aspects of structural analysis. It makes distinction between the constitutive and geometric parts of the element tangent stiffness, which could lead effortlessly to the non-linear effects associated with large displacements. The third is the hybrid Trefftz FEM (or T-Trefftz method) [4, 6]. Unlike in the conventional and natural FEM, the T-Trefftz method couples the advantages of FEM [1, 9] and BEM [10]. In contrast to the first two methods, the T-Trefftz method is based on a hybrid method which includes the use of an independent auxiliary inter-element frame field defined on each element boundary and an independent internal field chosen so as to a prior satisfy the homogeneous governing differential equations by means of a suitable truncated T-complete function set of homogeneous solutions. The final is the hybrid FEM based on the fundamental solution, F-Trefftz method for short [7, 11, 12]. The F-Trefftz method is significantly different from the previous three types mentioned above. In this method, a linear combination of the fundamental solution at different points is used to approximate the field variable within the element. The independent frame field defined along the element boundary and the newly developed variational functional are employed to guarantee the inter-element continuity, generate the final stiffness equation and establish linkage between the boundary frame field and internal field in the element. This review will focus on the last two methods.

It is noted that the T-Trefftz model, originating nearly forty years ago [4, 13], has been considerably improved and has now become a highly efficient computational tool for the solution of complex boundary value problems. In contrast to conventional FE models, the class of finite elements associated with the Trefftz method is based on a hybrid method which includes the use of an auxiliary inter-element displacement or traction frame to link the internal displacement fields of the elements. Such internal fields, chosen so as to a

priori satisfy the governing differential equations, have conveniently been represented as the sum of a particular integral of non-homogeneous equations and a suitably truncated T-complete set of regular homogeneous solutions multiplied by undetermined coefficients. Inter-element continuity is enforced by using a modified variational principle together with an independent frame field defined on each element boundary. The element formulation, during which the internal parameters are eliminated at the element level, leads to the standard force-displacement relationship, with a symmetric positive definite stiffness matrix. Clearly, while the conventional FE formulation may be assimilated to a particular form of the Rayleigh-Ritz method, the HT FE approach has a close relationship with the Trefftz method [6, 14]. As noted in [6, 15], the main advantages stemming from the HT FE model are: (a) the formulation calls for integration along the element boundaries only, which enables arbitrary polygonal or even curve-sided elements to be generated. As a result, it may be considered as a special, symmetric, substructure-oriented boundary solution approach and thus possesses the advantages of the boundary element method (BEM). In contrast to conventional boundary element formulation, however, the HT FE model avoids the introduction of singular integral equations and does not require the construction of a fundamental solution which may be very laborious to build; (b) the HT FE model is likely to represent the optimal expansion bases for hybrid-type elements where inter-element continuity need not be satisfied, a priori, which is particularly important for generating a quasi-conforming plate bending element; (c) the model offers the attractive possibility of developing accurate crack-tip, singular corner or perforated elements, simply by using appropriate known local solution functions as the trial functions of intra-element displacements.

Since the first attempt to generate a general-purpose T-Trefftz formulation [4] in 1977, the Trefftz element concept has become increasingly popular and has been applied to potential problems [16-18], two-dimensional elastics [19], elastoplasticity [20, 21], fracture mechanics [22, 23], micromechanics analysis [24], problem with holes [25, 26], heat conduction [27, 28], thin plate bending [29-32], thick or moderately thick plates [33-37], three-dimensional problems [38], piezoelectric materials [39-41], and contact problems [42, 43]. On the other hand, the F-Trefftz method, newly developed recently [7, 44], has gradually become popular in the field of mechanical and physical engineering since it is initiated in 2009 [7, 14]. It has been applied to potential problems [18, 45], plane elasticity [44, 46], composites [11, 24, 47], piezoelectric materials [48-50], three-dimensional problems [51], functionally graded materials [12, 52, 53], human eye problems [54, 55], Nanocomposites [56], hole problems [57, 58], crack problems [59], and skin burn problems [60, 61].

Following this introduction, the present review consists of six sections. T-Trefftz FEM nonlinear problems of minimal surface are described in Section 2. Section 3 focuses on the essentials of F-Trefftz elements for composites based on fundamental solutions and the modified variational principle appearing. It describes in detail the method of deriving element stiffness equations. The applications of F-Trefftz elements to functionally graded materials and skin tissues are discussed in Sections 4-5. Finally, a brief summary of the developments of the Treffz methods is provided and areas that need further research are identified.

II. T-Trefftz method for nonlinear problems of minimal surface

This section is concerned with the application of the T-Trefftz to the solution of nonlinear potential flow problems. By nonlinear potential problems we mean here soap bubble problems, also known as minimal surfaces problems or Plateau's problems, which are defined when the mean curvature is identically zero at any point on a smooth surface.

II.1 Statement of minimal surfaces

The minimal surfaces or soap bubble problem is to find a twice continuous differentiable function $u(x,y)$ in a region constrained by bounding contours which minimize the surface area functional:

$$A=\int_{\Omega}\sqrt{1+u_{,x}^2+u_{,y}^2}\,\mathrm{d}\Omega \qquad (1)$$

where a comma followed by a subscript represents differentiation.

The differential equation of this surface area problem is obtained using the Euler-Lagrange condition for minimization of the above functional. This yields the following nonlinear boundary value problem (BVP) for the determination of minimal surface

$$(1+u_{,y}^2)u_{,xx}-2u_{,x}u_{,y}u_{,xy}+(1+u_{,x}^2)u_{,yy}=0 \text{ in } \Omega \qquad (2)$$

subjected to the Dirichlet boundary condition

$$u = \bar{u}(x, y) \quad \text{on } \Gamma \tag{3}$$

where Ω is a strictly two-dimensional convex domain in R^2 and Γ is its boundary. It is sufficient to assume that the solution to Eq. (2) is unique if $\bar{u}(x, y)$, satisfying the bounded slope condition, is the restriction to Γ of a function in the Sobolev space for certain conditions [62].

Eq. (2) is of the elliptic type because its discriminant, namely $(1+u_{,x}^2)(1+u_{,y}^2)-u_{,x}^2u_{,y}^2$, is greater than zero.

Note that Eq. (2) describes the shape of a uniformly stretched membrane in the absence of transverse loads when it is bounded by one or more non-intersecting skew space contours in structural analysis. When the slopes are sufficiently small, their squares and products can be neglected and Eq. (2) can reduce to the classical Laplace equation

$$\nabla^2 u = u_{,xx} + u_{,yy} = 0 \tag{4}$$

which is the linearized equation of the unloaded membrane.

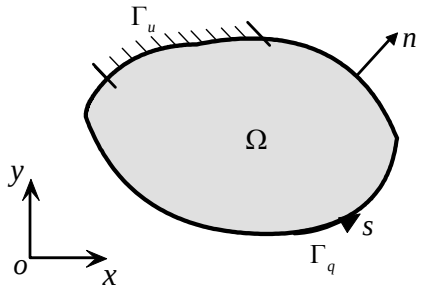

Fig. 1 Geometrical definitions and boundary conditions for general nonlinear potential problem

II.2 Solution procedure

To make the solution procedure below more popular and general, we consider a two dimensional generalized nonlinear second order BVP (see Fig. 1)

$$\Re(u, u_{,x}, u_{,y}, u_{,xx}, u_{,yy}, u_{,xy}) = g(x, y) \quad \text{in}\,\Omega \tag{5}$$

with the following boundary conditions

$$u = \bar{u} \qquad \text{on } \Gamma_u \tag{6}$$

$$q = \frac{\partial u}{\partial n} = \bar{q} \quad \text{on } \Gamma_q \tag{7}$$

where $\Re()$ denotes the general differential operator defined in a plane domain Ω bounded by the boundary Γ (see Fig. 1), $g(x, y)$ is a known function in terms of coordinates *x* and *y*, n is the normal to the boundary and $\bar{u}$ and $\bar{q}$ are specified single-value functions on the boundary.

The solution to the BVP defined by Eqs. (5)-(7) is, in general, very complicated due to its nonlinearity. In this section, a general T-Trefftz finite element approach with radial basis function interpolation is described to solve this category of nonlinear problems. The detailed process is presented below.

II.2.1 The concept of the analogue equation [63]

Suppose that $u = u(x, y)$ is the sought solution to the BVP described by Eqs. (5)-(7), which is twice continuously differentiable in the domain Ω. If the linear Laplacian operator is applied to this function, that is,

$$\nabla^2 u(x, y) = b(x, y) \quad \text{in } \Omega \tag{8}$$

we can see that Eq. (8) implies that a linear equivalent to the nonlinear Eq. (5) is produced. The solutions of Eqs. (5)-(7) can be established by solving this linear equation (8) under the same boundary conditions (6) and (7). Obviously, the fictitious source distribution $b(x, y)$ is related to the unknown function u and an iterative process is described as follows to deal with this obstacle.

II.2.2 The method of particular solution and radial basis function approximation

Since Eq. (8) is linear (if the fictitious source term $b(x, y)$ is viewed as a known function), its corresponding solution can be divided into two parts, a homogeneous solution $u_h(x, y)$ and a particular solution $u_p(x, y)$, that is

$$u = u_h + u_p \tag{9}$$

Accordingly, they should respectively satisfy

$$\nabla^2 u_p = b(x, y) \text{ in } \Omega \tag{10}$$

and

$$\nabla^2 u_h = 0 \qquad \text{in } \Omega \tag{11}$$

with modified boundary conditions

$$u_h = \bar{u}_h = \bar{u} - u_p \qquad \text{on } \Gamma_u \tag{12}$$

$$q_h = \bar{q}_h = \bar{q} - q_p \qquad \text{on } \Gamma_q \tag{13}$$

where $q_h = \frac{\partial u_h}{\partial n}$ and $q_p = \frac{\partial u_p}{\partial n}$.

From above equations we can see that, once the particular solution $u_p(x, y)$ fulfilling Eq. (10) is chosen, the homogeneous solution $u_h(x, y)$ is unique.

For the fictitious source distribution $b(x, y)$, we assume that [14, 64]

$$b(x,y)=\sum_{j=1}^{L}\alpha_j f_j(x,y)=\mathbf{f}\boldsymbol{\alpha} \tag{14}$$

where L is the number of interpolation points, f_j denotes the basis function used for interpolation, and α_j represents the set of interpolating coefficients.
Theoretically, any basis function can be used for interpolation. However, radial basis functions have been found to be most suitable for interpolating the fictitious source $b(x,y)$ [65, 66]. In most numerical analyses, the commonly used RBFs are

- Linear polynomial: $f_j=1+r_j$
- thin plate spline (TPS): $f_j=r_j^2\ln r_j$
- multiquadric (MQ): $f_j=\sqrt{r_j^2+c^2}$

where r_j represents the Euclidean distance of the given point (x,y) from a fixed point (x_j,y_j) in the domain of interest.
At the same time, it is reasonable to assume

$$u_p(x,y)=\sum_{j=1}^{L}\alpha_j\hat{u}_j=\hat{\mathbf{u}}\boldsymbol{\alpha} \tag{15}$$

$$q_p(x,y)=\frac{\partial u_p}{\partial n}=\sum_{j=1}^{L}\alpha_j\hat{q}_j=\hat{\mathbf{q}}\boldsymbol{\alpha}\quad(\hat{q}_j=\frac{\partial\hat{u}_j}{\partial n}) \tag{16}$$

if a relationship between f_j and $\hat{u}_j$ such as

$$\nabla^2\hat{u}_j=f_j \tag{17}$$

exists.
Since the fictitious source distribution $b(x,y)$ is determined by the unknown function u, the particular solution and its normal derivative cannot be directly determined using the formulation in this section. However, this formulation still contributes to constructing the approximated expression of the unknown function u.

II.2.3 Trefftz finite element method

In this section, we apply the theory of T-Trefftz FEM [6] to the homogeneous linear BVP consisting of Eqs. (11)-(13).

For a particular element, say element e, we assume two fields:

(a) The non-conforming intra-element field

$$u_{eh}(x,y)=\sum_{j=1}^{m}N_{ej}c_{ej}=\mathbf{N}_e\mathbf{c}_e \tag{18}$$

where $\mathbf{c}_e$ is a vector of undetermined coefficients and m is its number of components. N_{ej} are homogeneous solutions to Eq. (11) obtained by a suitably truncated T-complete solution. For example,

$$N_{e(2n-1)}=r_e^n\cos n\theta_e,\ N_{e(2n)}=r_e^n\sin n\theta_e\quad(n=1,2,\cdots) \tag{19}$$

for a two dimensional problem with a bounded domain. With regard to the proper number m of trial functions N_{ej} for the element, the basic rule used to prevent spurious energy modes is analogous to that in the hybrid-stress model. The necessary (but not sufficient) condition is stated as[6]

$$m\ge k-r \tag{20}$$

where k is the number of nodal DOF of the element under consideration and r represents the discarded rigid body motion terms. For instance, $r=1$ in the Poisson equation and $r=3$ in the 2D linear elastic case.

Additionally, the corresponding outward normal derivative of u_{eh} on Γ_e is

$$q_{eh}=\frac{\partial u_{eh}}{\partial n}=\mathbf{T}_e\mathbf{c}_e \tag{21}$$

where $\mathbf{T}_e=\frac{\partial\mathbf{N}_e}{\partial n}$.

(b) An auxiliary conforming frame field

In order to enforce on u_h the conformity, for instance, $u_{eh}=u_{fh}$ on $\Gamma_e\cap\Gamma_f$ of any two neighboring elements, we use an auxiliary inter-element frame field $\tilde{u}_h$ approximated in terms of the same degrees of freedom (DOF), $\mathbf{d}$, as used with the conventional elements. In this case, as standard HT element, $\tilde{u}_h$ is confined to the whole element boundary, that is,

$$\tilde{u}_{eh}(x,y)=\tilde{\mathbf{N}}_e\mathbf{d}_e \tag{22}$$

which is independently assumed along the element boundary in terms of nodal degree of freedom (DOF) $\mathbf{d}_e$, where $\tilde{\mathbf{N}}_e$ represents the conventional finite element interpolating functions. For example, a simple interpolation of the frame field on the side 2-3 of a particular element (Fig. 2) can be given in the form

$$\tilde{u}_{23}=\tilde{N}_1u_2+\tilde{N}_2u_3 \tag{23}$$

where

$$\tilde{N}_1=\frac{1-\xi}{2},\quad\tilde{N}_2=\frac{1+\xi}{2} \tag{24}$$

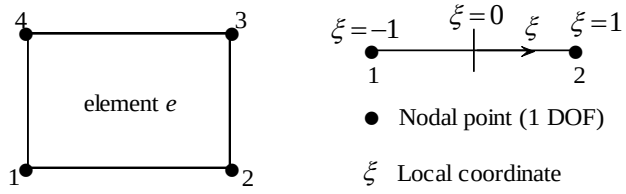

Fig. 2 Typical two-dimensional 4-node element with linear frame function

(c) Jirousek's variational principle [4, 6]

The variational functional Π corresponding to the whole system can be written as the sum of E element quantities Π_e as

$$\Pi = \sum_{e=1}^{E} \Pi_e \tag{25}$$

where E is the total number of elements, and Π_e is the variational functional related to a particular element e, which is expressed as [14]

$$\begin{aligned} \Pi_e = &-\frac{1}{2}\int_{\Omega_e} (q_1^2 + q_2^2)\mathrm{d}\Omega - \int_{\Gamma_{eu}} q_h \bar{u}_h \mathrm{d}\Gamma \\ &+ \int_{\Gamma_{eq}} \left(\bar{q}_h - q_h\right)\tilde{u}_h \mathrm{d}\Gamma - \int_{\Gamma_{eI}} q_h \tilde{u}_h \mathrm{d}\Gamma \end{aligned} \tag{26}$$

where Ω_e stands for the eth element sub-domain, $\Gamma_e = \Gamma_{eu} + \Gamma_{eq} + \Gamma_{eI}$, with $\Gamma_{eu} = \Gamma_e \cap \Gamma_u$, $\Gamma_{eq} = \Gamma_e \cap \Gamma_q$, and Γ_{eI} is the inter-element boundary of element e.

Integrating the domain integral term in Eq. (23) by parts, we obtain

$$\begin{aligned} \Pi_e = &\frac{1}{2}\int_{\Gamma_e} q_h u_h \mathrm{d}\Gamma - \int_{\Gamma_{eu}} q_h \bar{u}_h \mathrm{d}\Gamma \\ &+ \int_{\Gamma_{eq}} \left(\bar{q}_h - q_h\right)\tilde{u}_h \mathrm{d}\Gamma - \int_{\Gamma_{eI}} q_h \tilde{u}_h \mathrm{d}\Gamma \end{aligned} \tag{27}$$

Substituting Eqs. (18), (21) and (22) into the functional (27) produces

$$\Pi_e = -\frac{1}{2}\mathbf{c}_e{}^{\mathrm{T}}\mathbf{H}_e\mathbf{c}_e + \mathbf{c}_e{}^{\mathrm{T}}\mathbf{S}_e\mathbf{d}_e + \mathbf{c}_e{}^{\mathrm{T}}\mathbf{r}_{1e} + \mathbf{d}_e{}^{\mathrm{T}}\mathbf{r}_{2e} \tag{28}$$

where

$$\mathbf{H}_e = -\int_{\Gamma_e} \mathbf{T}_e{}^{\mathrm{T}}\mathbf{N}_e \mathrm{d}\Gamma$$

$$\mathbf{S}_e = -\int_{\Gamma_{eq}\cup\Gamma_{eI}} \mathbf{T}_e{}^{\mathrm{T}}\tilde{\mathbf{N}}_e \mathrm{d}\Gamma$$

$$\mathbf{r}_{1e} = -\int_{\Gamma_{eu}} \mathbf{T}_e{}^{\mathrm{T}}\bar{u}_h \mathrm{d}\Gamma = -\int_{\Gamma_{eu}} \mathbf{T}_e{}^{\mathrm{T}}\left(\bar{u} - \hat{\mathbf{u}}\boldsymbol{\alpha}\right)\mathrm{d}\Gamma = \mathbf{r}_{1e}(\boldsymbol{\alpha})$$

$$\mathbf{r}_{2e} = \int_{\Gamma_{eq}} \tilde{\mathbf{N}}_e{}^{\mathrm{T}}\bar{q}_h \mathrm{d}\Gamma = \int_{\Gamma_{eq}} \tilde{\mathbf{N}}_e{}^{\mathrm{T}}\left(\bar{q} - \hat{\mathbf{q}}\boldsymbol{\alpha}\right)\mathrm{d}\Gamma = \mathbf{r}_{2e}(\boldsymbol{\alpha})$$

For the minimization of the functional Π, using the necessary conditions

$$\frac{\partial \Pi}{\partial \mathbf{c}^{\mathrm{T}}} = \sum_{e=1}^{E} \frac{\partial \Pi_e}{\partial \mathbf{c}^{\mathrm{T}}} = \sum_{e=1}^{E} \frac{\partial \Pi_e}{\partial \mathbf{c}_e{}^{\mathrm{T}}} = \mathbf{0} \tag{29}$$

$$\frac{\partial \Pi}{\partial \mathbf{d}^{\mathrm{T}}} = \sum_{e=1}^{E} \frac{\partial \Pi_e}{\partial \mathbf{d}^{\mathrm{T}}} = \sum_{e=1}^{E} \frac{\partial \Pi_e}{\partial \mathbf{d}_e{}^{\mathrm{T}}} = \mathbf{0} \tag{30}$$

we can obtain

$$-\mathbf{H}\mathbf{c} + \mathbf{S}\mathbf{d} + \mathbf{r}_1 = \mathbf{0} \tag{31}$$

$$\mathbf{S}^{\mathrm{T}}\mathbf{c} + \mathbf{r}_2 = \mathbf{0} \tag{32}$$

where $\mathbf{c}$ and $\mathbf{d}$ are the total coefficients vector of T-complete functions interpolation and nodal unknowns related to the full system, respectively.

Eqs. (31) and (32) lead to

$$\mathbf{c} = \mathbf{G}\mathbf{d} + \mathbf{g} \tag{33}$$

$$\mathbf{K}\mathbf{d} = \mathbf{p}(\boldsymbol{\alpha}) \tag{34}$$

where $\mathbf{G} = \mathbf{H}^{-1}\mathbf{S}$, $\mathbf{g} = \mathbf{H}^{-1}\mathbf{r}_1$, $\mathbf{K} = \mathbf{G}^{\mathrm{T}}\mathbf{H}\mathbf{G}$ and $\mathbf{p} = -\mathbf{G}^{\mathrm{T}}\mathbf{H}\mathbf{g} - \mathbf{r}_2$.

Consequently, vectors $\mathbf{c}$ and $\mathbf{d}$ are expressed in terms of the unknown interpolation coefficient $\boldsymbol{\alpha}$ by means of Eqs. (33) and (34).

(d) Finding the discarded rigid body motion terms

It suffices to reintroduce the discarded modes in the internal field u_{eh} of a particular element and then to calculate their undetermined coefficients by requiring, for example, the least squares adjustment of u_{eh} and $\tilde{u}_{eh}$. In this case, these missing terms can easily be recovered by setting for the augmented internal field

$$u_{eh}(x, y) = \mathbf{N}_e\mathbf{c}_e + c_0 \tag{35}$$

and using a least-square procedure to match u_{eh} and $\tilde{u}_{eh}$ at nodes of the element boundary Γ_e:

$$\sum_{i=1}^{N_e} \left(u_{eh} - \tilde{u}_{eh}\right)^2\Big|_{node\ i} = \min \tag{36}$$

where N_e is the number of nodes for the element under consideration. The above equation finally yields

$$\sum_{i=1}^{N_e} \left(N_e c_e + c_0 - \tilde{u}_{eh}\right)\Big|_{node\ i} = 0 \tag{37}$$

Then, we have

$$c_0 = \frac{1}{N_e}\sum_{i=1}^{N_e} \left(\tilde{u}_{eh} - \mathbf{N}_e\mathbf{c}_e\right)\Big|_{node\ i} \tag{38}$$

II.2.4 Final nonlinear equations

At an arbitrary point (x, y) in element e, the full solution can be expressed as

$$u(x,y)=\hat{\mathbf{u}}\big|_{(x,y)}\boldsymbol{\alpha}+\mathbf{N}\big|_{(x,y)}\mathbf{c}+c_0=\mathbf{u}(\boldsymbol{\alpha}) \tag{39}$$

Furthermore, the related derivatives can also be obtained

$$u_{,x}(x,y)=\hat{\mathbf{u}}_{,x}\big|_{(x,y)}\boldsymbol{\alpha}+\mathbf{N}_{,x}\big|_{(x,y)}\mathbf{c}=\mathbf{u}_{,x}(\boldsymbol{\alpha}) \tag{40}$$

$$u_{,y}(x,y)=\hat{\mathbf{u}}_{,y}\big|_{(x,y)}\boldsymbol{\alpha}+\mathbf{N}_{,y}\big|_{(x,y)}\mathbf{c}=\mathbf{u}_{,y}(\boldsymbol{\alpha}) \tag{41}$$

$$u_{,xx}(x,y)=\hat{\mathbf{u}}_{,xx}\big|_{(x,y)}\boldsymbol{\alpha}+\mathbf{N}_{,xx}\big|_{(x,y)}\mathbf{c}=\mathbf{u}_{,xx}(\boldsymbol{\alpha}) \tag{42}$$

$$u_{,xy}(x,y)=\hat{\mathbf{u}}_{,xy}\big|_{(x,y)}\boldsymbol{\alpha}+\mathbf{N}_{,xy}\big|_{(x,y)}\mathbf{c}=\mathbf{u}_{,xy}(\boldsymbol{\alpha}) \tag{43}$$

$$u_{,yy}(x,y)=\hat{\mathbf{u}}_{,yy}\big|_{(x,y)}\boldsymbol{\alpha}+\mathbf{N}_{,yy}\big|_{(x,y)}\mathbf{c}=\mathbf{u}_{,yy}(\boldsymbol{\alpha}) \tag{44}$$

In order to determine the unknown coefficient $\boldsymbol{\alpha}$, it should be forced to satisfy the governing Eq. (2) at L interpolating points, that is

$$\Re(\boldsymbol{\alpha})\big|_{(x_i,y_i)}=g(x_i,y_i),\quad i=1,2,\cdots,L \tag{45}$$

from which the unknown coefficients vector $\boldsymbol{\alpha}$ can be determined by means of iterative algorithms.

It is clear that once all unknowns are determined, the distribution of field u at any point in the domain can be calculated using Eq. (39).

III. F-Trefftz methods for composites

III.1 Mathematical Model

A two-dimensional mathematical model of steady-state heat conduction in the cross-section of the unidirectional fiber-reinforced composites is considered in this section. The fibers in the composites are assumed to be infinite parallel and have a reasonably circular shape with a fairly uniform diameter. For the sake of convenience, since matrix and fiber occupy different regions, the regions occupied by the isotropic matrix and fiber inclusions are referred to as regions Ω_{M} and Ω_{F}, respectively, and the quantities associated with these regions are denoted by the corresponding subscripts M or F (see Figure 3).

It is well known that a representative volume cell (RVC) for real composites with the smallest periodic repeat volume is usually selected to study the effective properties of composites in the micromechanics analysis (see Figure 3). Without loss of generality, two-dimensional heat conduction problems in the square RVC with multiple fibers are considered, and the governing equations in terms of spatial variable $\mathbf{X}=(X_1,X_2)$ in matrix and fibers can respectively be written as

$$\begin{aligned} k_{\mathrm{M}}u_{\mathrm{M},ii}(\mathbf{X})&=0 \qquad \forall\mathbf{X}\in\Omega_{\mathrm{M}}\\ k_{\mathrm{F}}u_{\mathrm{F},ii}(\mathbf{X})&=0 \qquad \forall\mathbf{X}\in\Omega_{\mathrm{F}}\end{aligned} \tag{46}$$

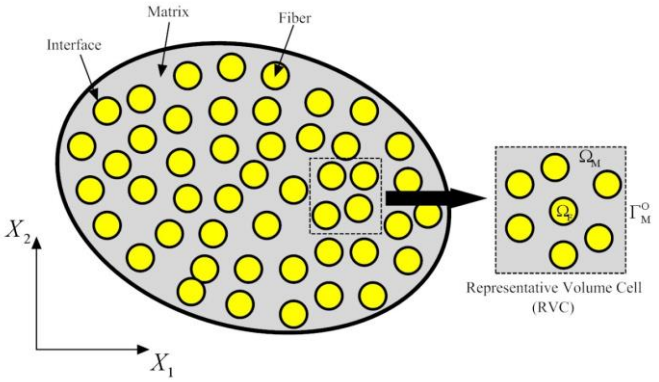

Figure 3 Geometrical definition for plane heat conduction problems in fiber-reinforced composites

with the following boundary conditions applied on the outer boundary $\Gamma_{\mathrm{M}}^{\mathrm{O}}=\Gamma_u\cup\Gamma_q\cup\Gamma_c$ of the matrix

$$\begin{cases} u_{\mathrm{M}}=\overline{u} & \text{on } \Gamma_u\\ q_{\mathrm{M}}=-k_{\mathrm{M}}u_{\mathrm{M},i}n_i=\overline{q} & \text{on } \Gamma_q\\ q_{\mathrm{M}}=h_{env}(u_{\mathrm{M}}-u_{env}) & \text{on } \Gamma_c\end{cases} \tag{47}$$

and the continuity conditions at the interface ($\Omega_{\mathrm{M}}\cap\Omega_{\mathrm{F}}$) between the fiber and the matrix for the case of perfect bonding

$$\begin{cases} u_{\mathrm{M}}=u_{\mathrm{F}}\\ q_{\mathrm{M}}+q_{\mathrm{F}}=0\end{cases} \tag{48}$$

where u_{M} and u_{F} are the temperature fields sought, k_{M} and k_{F} are the thermal conductivities and n_i is the i th component of the unit outward normal vector to the particular boundary. q_{M} and q_{F} represent the surface normal heat flux along the unit outward normal. $\overline{u}$ and $\overline{q}$ are specified functions on the corresponding boundaries. h_{env} is the convection heat-transfer coefficient or film coefficient, and u_{env} is the ambient environment temperature. The space derivatives are indicated by a comma, i.e. $u_{,i}=\partial u/\partial X_i$, and the subscript index i takes values 1 and 2 for the two-dimensional case. Additionally, the repeated subscript indices stand for the summation convention.

III.2 Fundamental solutions

Fundamental solutions play an important role in the derivation of the F-Trefftz FEM formulation. The fundamental solution represents the material response at an arbitrary point when a unit point source is applied at a

source point in an infinite domain. With the proposed F-Trefftz FEM, for plane heat conduction problems in fiber-reinforced composites, two types of fundamental solution are used. One is the temperature response in an infinite matrix region Ω_M ($|z| \geq 0$) in the absence of fibers (see Figure 4a), and the other is the temperature response in an infinite matrix region Ω_M ($|z| > R$) containing a circular fiber Ω_F ($|z| < R$) (Figure 4b), where $z = x_1 + x_2 i$ is a complex number defined in a local coordinate system $\mathbf{x} = (x_1, x_2)$ with its origin coincident with the fiber center, and $i = \sqrt{-1}$ denotes the unit imaginary number.

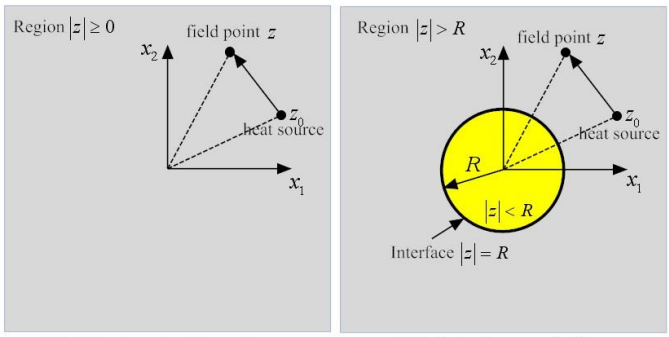

(a) Infinite domain without fiber (b) Infinite domain with fiber

Fig. 4 Fundamental solutions for plane heat conduction problems in fiber-reinforced composites

III.2.1 Fundamental solution without fiber

For the case of an infinite domain without fibres, assuming that a unit heat source is located at point z_0 in the infinite matrix domain Ω_M (Figure 4a), the temperature response G_M at any field point z is given in the form [67]

$$G_M(z, z_0) = -\frac{1}{2\pi k_M} \mathrm{Re}\{\ln(z - z_0)\} \qquad (49)$$

where Re denotes the real part of the bracketed expression. Clearly, the expression (49) shows singularity as $z = z_0$, which is the inherent feature of the fundamental solution.

III.2.2Fundamental solution with fiber

For the case of an infinite domain with a centered circular fiber, consider a unit heat source located at the source point z_0 in the infinite matrix Ω_M (Figure 4b). Then the temperature responses G_M and G_F at any field point z in matrix and fiber regions are respectively obtained as [67]

$$\begin{cases} G_M = -\dfrac{1}{2\pi k_M}\left[\mathrm{Re}[\ln(z - z_0)] + \dfrac{k_M - k_F}{k_M + k_F} \times \mathrm{Re}[\ln(\dfrac{R^2}{z} - \overline{z}_0)]\right] & z \in \Omega_M \\ G_F = -\dfrac{1}{(k_M + k_F)\pi}\mathrm{Re}[\ln(z - z_0)] & z \in \Omega_F \end{cases} \qquad (50)$$

using the complex potential theory and introducing the continuity condition (48) in the interface $|z| = R$. Similarly, the induced temperature G_M in the matrix shows a proper singular behavior at the source point z_0, while G_F in the fiber is regular because the source point z_0 is outside the fiber. Additionally, it is worth noting that since the fundamental solutions already include the presence of interface between the fillers and matrix, it's not necessary to model the temperature and heat flux continuity condition on the interface and then the analysis will become simpler. This is one of advantages of the proposed approach stated below.

III.3 The hybrid finite element formulation

In this section, the formulation of the hybrid finite element model with fundamental solution as an interior trial function is presented for heat analysis of two-dimensional fiber-reinforced composites.

III.3.1 Non-conforming intra-element field

Applying the method of fundamental solution (MFS) [68] to remove the singularity of the fundamental solution, for a particular element, say element e, occupying a sub-domain Ω_e embedded with a centered circular fiber of radius R and defined in a local reference system $\mathbf{x} = (x_1, x_2)$ whose axis remains parallel to the axis of the global reference system $\mathbf{X} = (X_1, X_2)$ (see Figure 5), the temperature field at any point $\mathbf{x}$ within the element domain is assumed to be a linear combination of fundamental solutions centered at different source points $\mathbf{x}_{sj}$, that is,

$$u_e(\mathbf{x}) = \sum_{j=1}^{n_s} G_e(\mathbf{x}, \mathbf{x}_{sj}) c_{ej} = \mathbf{N}_e(\mathbf{x}) \mathbf{c}_e \qquad (51)$$

where c_{ej} represents undetermined coefficients, n_s is the number of virtual sources outside the element e, and

$G_e(\mathbf{x},\mathbf{x}_{sj})$ represents the corresponding fundamental solution, which can be conveniently expressed using a unified form

$$G_e(\mathbf{x},\mathbf{x}_{sj})=\begin{cases}G_{\mathrm{M}}(\mathbf{x},\mathbf{x}_{sj}) & \mathbf{x}\in\Omega_{\mathrm{M}}\\ G_{\mathrm{F}}(\mathbf{x},\mathbf{x}_{sj}) & \mathbf{x}\in\Omega_{\mathrm{F}}\end{cases} \tag{52}$$

In practice, the location of sources affects the final accuracy [69-71] and can usually be determined by means of the formulation [72]

$$\mathbf{x}_s=\mathbf{x}_b+\gamma\left(\mathbf{x}_b-\mathbf{x}_c\right) \tag{53}$$

where γ is a dimensionless coefficient, $\mathbf{x}_b$ is the elementary boundary point and $\mathbf{x}_c$ the geometrical centroid of the element. For a particular element as shown in Figure 5, we can use the nodes of element to generate related source points using the relation (8).

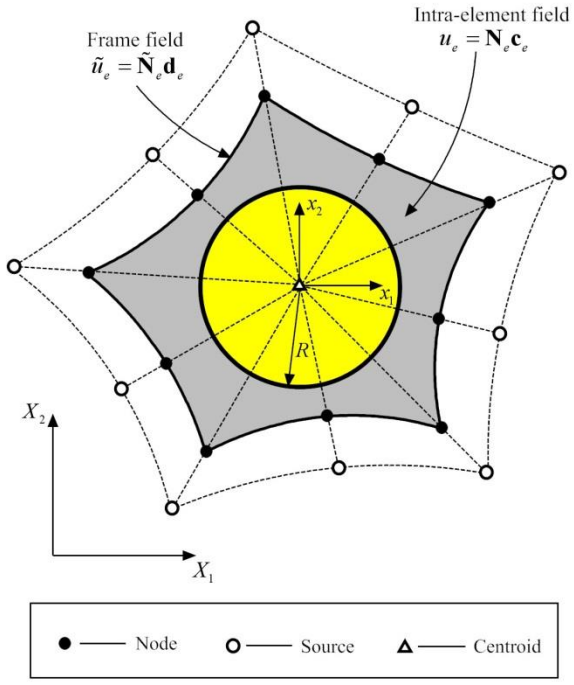

Fig. 5 Intra-element field, frame field in a particular element in HFS-FEM, and the generation of source points for a particular inclusion element

The corresponding outward normal derivative of u_e on Γ_e is defined by

$$q_e=-k_M\frac{\partial u_e}{\partial n}=\mathbf{Q}_e\mathbf{c}_e \tag{54}$$

where

$$\mathbf{Q}_e=-k_M\frac{\partial\mathbf{N}_e}{\partial n}=-k_M\mathbf{A}\mathbf{T}_e \tag{55}$$

with

$$\mathbf{A}=\begin{bmatrix}n_1 & n_2\end{bmatrix},\quad \mathbf{T}_e=\begin{bmatrix}\dfrac{\partial\mathbf{N}_e}{\partial x_1} & \dfrac{\partial\mathbf{N}_e}{\partial x_2}\end{bmatrix}^{\mathrm{T}} \tag{56}$$

III.3.2 Auxiliary conforming frame field

In order to enforce conformity on the field variable u, for instance, $u_e=u_f$ on $\Gamma_e\cap\Gamma_f$ of any two neighboring elements *e* and *f*, an auxiliary inter-element frame field $\tilde{u}$ independent of the intra-element field is introduced in terms of the same nodal degrees of freedom (DOF), $\mathbf{d}$, as used in conventional finite element methods. In this case, $\tilde{u}$ is confined to the whole element boundary, that is

$$\tilde{u}_e(\mathbf{x})=\tilde{\mathbf{N}}_e(\mathbf{x})\mathbf{d}_e \tag{57}$$

where $\tilde{\mathbf{N}}_e$ represents the conventional finite element interpolating functions. For example, a simple interpolation of the frame field on any side of a particular element (Fig. 6) can be given in the form

$$\tilde{u}=\tilde{N}_1u_1+\tilde{N}_2u_2+\tilde{N}_3u_3 \tag{58}$$

where $\tilde{N}_i$ ($i=1,2,3$) stands for shape functions in terms of natural coordinate ξ defined in Fig. 6.

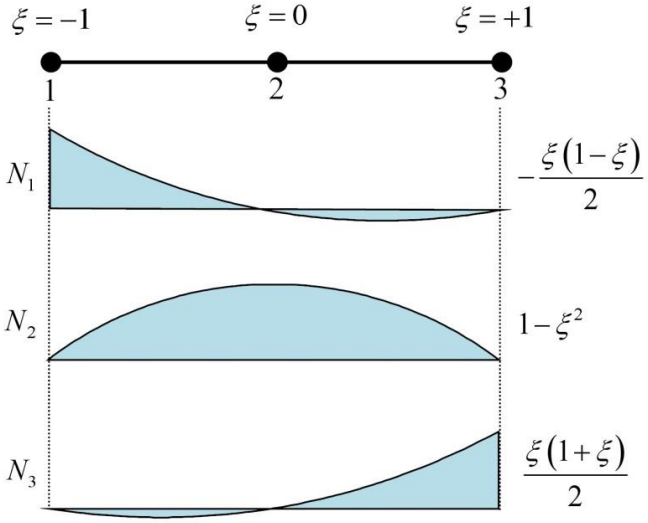

Fig. 6 Typical quadratic interpolation for the frame field

III.4 Modified variational principle and stiffness equation

For the boundary value problem defined in Eqs (1)-(2), since the stationary conditions of the traditional potential or complementary variational functional cannot guarantee the satisfaction of the continuity condition on the inter-element boundary, which is required in the proposed hybrid finite element model, a modified potential functional [7] is developed as follows

$$\Pi_m = \sum_e \Pi_{me} \tag{59}$$

with

$$\Pi_{me} = -\frac{1}{2}\int_{\Omega_e} k u_{,i} u_{,i} \mathrm{d}\Omega - \int_{\Gamma_{qe}} \bar{q}\tilde{u}\mathrm{d}\Gamma + \int_{\Gamma_e} q(\tilde{u}-u)\mathrm{d}\Gamma \tag{60}$$

in which the governing equation (46) is assumed to be satisfied, *a priori*, due to the use of the fundamental solution in the F-Trefftz FE model. The boundary Γ_e of a particular element consists of the following parts

$$\Gamma_e = \Gamma_{ue} \cup \Gamma_{qe} \cup \Gamma_{Ie} \tag{61}$$

where Γ_{Ie} represents the inter-element boundary of the element 'e'.

Appling the divergence theorem

$$\int_\Omega f_{,i} h_{,i} \mathrm{d}\Omega = \int_\Gamma h f_{,i} n_i \mathrm{d}\Gamma - \int_\Omega h\nabla^2 f \mathrm{d}\Omega \tag{62}$$

for any smooth functions f and h in the domain, we can eliminate the domain integral from Eq. (60) and obtain following functional for the F-Trefftz model

$$\Pi_{me} = -\frac{1}{2}\int_{\Gamma_e} q u \mathrm{d}\Gamma - \int_{\Gamma_{qe}} \bar{q}\tilde{u}\mathrm{d}\Gamma + \int_{\Gamma_e} q\tilde{u}\mathrm{d}\Gamma \tag{63}$$

Then, substituting Eqs. (51), (54) and (57) into the functional (63) produces

$$\Pi_e = -\frac{1}{2}\mathbf{c}_e{}^{\mathrm{T}}\mathbf{H}_e\mathbf{c}_e - \mathbf{d}_e{}^{\mathrm{T}}\mathbf{g}_e + \mathbf{c}_e{}^{\mathrm{T}}\mathbf{G}_e\mathbf{d}_e \tag{64}$$

in which

$$\mathbf{H}_e = \int_{\Gamma_e} \mathbf{Q}_e^{\mathrm{T}}\mathbf{N}_e \mathrm{d}\Gamma,\ \mathbf{G}_e = \int_{\Gamma_e} \mathbf{Q}_e^{\mathrm{T}}\tilde{\mathbf{N}}_e \mathrm{d}\Gamma,\ \mathbf{g}_e = \int_{\Gamma_{eq}} \tilde{\mathbf{N}}_e^{\mathrm{T}}\bar{q}\mathrm{d}\Gamma$$

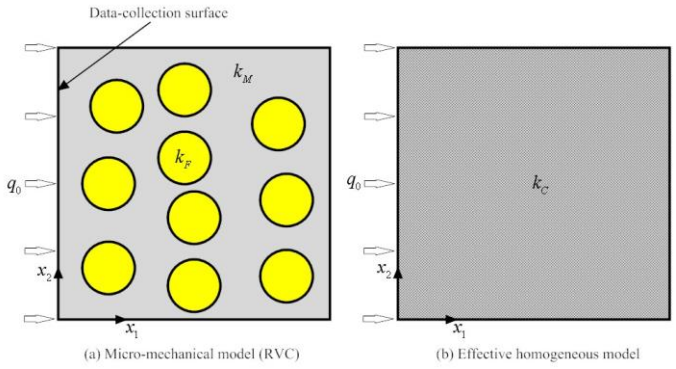

Fig. 7 Micro-mechanical model (RVC) and effective homogeneous model

III.5 Effective thermal conductivity

The effective thermal conductivity is a very important parameter for engineering applications of composites. Usually the RVC approach is utilized in micro-mechanical model development. In this paper, a general square RVC with random multiple inclusions is used to investigate the effect of fiber size and to evaluate the effective thermal properties for the case of two-dimensional heat conduction (see Fig. 7a). The side length of the RVC is taken to be L. Meanwhile, an effective homogeneous model with the same geometry as the RVC is assumed with constant effective thermal conductivity k_C.

According to Fourier's law, the thermal conductivity along the $i-$direction is defined as

$$k_i = -\frac{q_i}{(\partial u / \partial x_i)} \tag{65}$$

Therefore the effective thermal conductivity of the equivalent homogeneous model (Fig. 7b) can be computed by applying appropriate boundary conditions. For example, in the homogeneous model, if (a) a uniform heat flux q_0 is horizontally applied on the left side of the square; (b) the temperature on the right side remains zero, (c) both the top and bottom sides are insulated, then, the temperature distribution in the model is linear in the horizontal direction; and the heat flux component in the body is constant, subsequently, the effective thermal conductivity k_c in the horizontal direction can be evaluated by the following formula

$$k_C = -\frac{q_0}{(\partial u / \partial x_1)} = -\frac{q_0}{(\Delta u / \Delta x_1)} = -\frac{q_0}{(u_{left} / L)} \tag{66}$$

where Δu is the temperature difference between the left and right surfaces and u_{left} represents the temperature on the left surface.

On the basis of the above discussion, the effective thermal conductivity can be estimated from the real RVC with multiple fibers by applying the same boundary conditions as those applied in the effective model, and using the temperature results on the left and right, two data-collection sides, that is,

$$k_C = -\frac{q_0}{(\tilde{u}_{left} / L)} \tag{67}$$

where $\tilde{u}_{left}$ is the average temperature on the left data-collection surface, which can be evaluated from nodal temperatures obtained by the presented hybrid finite element formulation.

IV. F-Trefftz methods for functionally graded materials

IV.1 Basic formulations

Consider a two-dimensional (2D) heat conduction

problem defined in an anisotropic inhomogeneous media:

$$\sum_{i,j=1}^{2}\frac{\partial}{\partial X_i}(\tilde{K}_{ij}(\mathbf{X},\mathrm{u})\frac{\partial u(\mathbf{X})}{\partial X_j})=0 \qquad \forall \mathbf{X}\in\Omega \quad (68)$$

For an inhomogeneous nonlinear functionally graded material, we assume the thermal conductivity varies exponentially with position vector and also be a function of temperature, that is

$$\tilde{K}_{ij}(\mathbf{X},u)=\alpha(u)K_{ij}\exp(2\boldsymbol{\beta}\cdot\mathbf{X}) \quad (69)$$

where $\alpha(u)>0$ is a function of temperature which may be different for different materials, the vector $\boldsymbol{\beta}=(\beta_1,\beta_2)$ is a dimensionless graded parameter and matrix $\mathbf{K}=[K_{ij}]_{1\le i,j\le 2}$ is a symmetric, positive-definite constant matrix ($K_{12}=K_{21}, \det K=K_{11}K_{22}-K_{12}{}^2>0$).

The boundary conditions are as follows:

—Dirichlet boundary condition

$$u=\bar{u} \qquad \text{on } \Gamma_u \quad (70)$$

—Neumann boundary condition

$$q=-\sum_{i,j=1}^{2}\tilde{K}_{ij}\frac{\partial u}{\partial X_j}n_i=\bar{q} \qquad \text{on } \Gamma_q \quad (71)$$

where $\tilde{K}_{ij}$ denotes the thermal conductivity which is the function of spatial variable $\mathbf{X}$ and unknown temperature field u. q represents the boundary heat flux. n_j is the direction cosine of the unit outward normal vector $\mathbf{n}$ to the boundary $\Gamma=\Gamma_u\cup\Gamma_q$. $\bar{u}$ and $\bar{q}$ are specified functions on the related boundaries, respectively.

IV.2 Kirchhoff transformation and iterative method

Two methods are employed here to deal with the nonlinear term $\alpha(u)$, one is Kirchhoff transformation [73] and another is the iterative method.

(1) Kirchhoff transformation

$$\Psi(u)=\psi(u(\mathbf{X}))=\int\alpha(u)du \quad (72)$$

Making use of Eq.(5), Eq.(1) reduces to

$$\sum_{i,j=1}^{2}\frac{\partial}{\partial X_i}(K_{ij}^{*}(\mathbf{X})\frac{\partial\Psi(\mathbf{X})}{\partial X_j})=0 \quad \forall\mathbf{X}\in\Omega \quad (73)$$

where

$$K_{ij}^{*}(\mathbf{X})=K_{ij}\exp(2\boldsymbol{\beta}\cdot\mathbf{X}) \quad (74)$$

Substituting Eq.(74) into Eq.(73) yields

$$\left[\sum_{i,j=1}^{2}K_{ij}\frac{\partial^2\Psi(\mathbf{X})}{\partial X_i\partial X_j}+2\boldsymbol{\beta}\cdot(\mathbf{K}\nabla\Psi(\mathbf{X}))\right]\exp(2\boldsymbol{\beta}\cdot\mathbf{X})=0 \quad (75)$$

where

$$u=\psi^{-1}(\Psi) \quad (76)$$

It should be mentioned that the inverse of Ψ in Eq.(76) exists since $\alpha(u)>0$.

The fundamental solution to Eq.(75) in two dimensions can be expressed as [73, 74]

$$N(\mathbf{X},\mathbf{X}_s)=-\frac{K_0(\kappa R)}{2\pi\sqrt{\det\mathbf{K}}}\exp\{-\boldsymbol{\beta}\cdot(\mathbf{X}+\mathbf{X}_s)\} \quad (77)$$

where $\kappa=\sqrt{\boldsymbol{\beta}\cdot\mathbf{K}\boldsymbol{\beta}}$, R is the geodesic distance defined as $R=R(\mathbf{X},\mathbf{X}_s)=\sqrt{\mathbf{r}\cdot\mathbf{K}^{-1}\mathbf{r}}$ and $\mathbf{r}=\mathbf{X}-\mathbf{X}_s$ in which $\mathbf{X}$ and $\mathbf{X}_s$ denote observing field point and source point in the infinite domain, respectively. K_0 is the modified Bessel function of the second kind of zero order. For isotropic materials, $K_{12}=K_{21}=0$, $K_{11}=K_{22}=k_0>0$, then the fundamental solution given by (77) reduces to

$$N(\mathbf{X},\mathbf{X}_s)=-\frac{K_0(\kappa R)}{2\pi k_0}\exp\{-\boldsymbol{\beta}\cdot(\mathbf{X}+\mathbf{X}_s)\} \quad (78)$$

which agrees with the result in [75].

Under the Kirchhoff transformation, the boundary conditions (70)-(71) are transformed into the corresponding boundary conditions in terms of Ψ.

$$\Psi=\psi(\bar{u}) \quad \text{on } \Gamma_u \quad (79)$$

$$p=-\sum_{i,j=1}^{2}K_{ij}^{*}\frac{\partial\Psi}{\partial X_j}n_i=-\sum_{i,j=1}^{2}\tilde{K}_{ij}\frac{\partial u}{\partial X_j}n_i=q=\bar{q} \text{ on } \Gamma_q \quad (80)$$

Therefore, by Kirchhoff transformation, the original nonlinear heat conduction equation (68), in which the heat conductivity is a function of coordinate X and unknown function u, can be transformed into the linear equation (73) in which the heat conductivity is just a function of coordinate X. At the same time, the field variable becomes Ψ in Eq.(73), rather than u in Eq.(68). The boundary conditions (70)-(71) are correspondingly transformed into Eqs.(79)-(80). Once Ψ is determined, the temperature solution u can be found by the reversion of transformation (76), i.e. $u=\psi^{-1}(\Psi)$.

(2) Iterative method

Since the heat conductivity depends on the unknown function u, an iterative procedure is employed for determining the temperature distribution. The algorithm

is given as follows:

1. Assume an initial temperature u^0.
2. Calculate the heat conductivity in Eq.(69) using u^0.
3. Solve the boundary value problem defined by Eqs.(68)-(71) for the temperature *u*
4. Define the convergent criterion $\left|u-u^0\right|<\delta$ ($\delta=10^{-6}$ in our analysis). If the criterion is satisfied, output the result and terminate the process. If not satisfied, go to next step.
5. Update u^0 with u
6. Go to step 2.

IV.3 Generation of graded element

In this section, an element formulation is presented to deal with materials with continuous variation of physical properties. Such an element model is usually known as a hybrid graded element which can be used for solving the boundary value problem (BVP) defined in Eqs.(73) and (79)-(80).

The proposed approach is based on a hybrid finite element formulation in which fundamental solutions are taken as intra-element interpolation functions [7]. Similar to HT-FEM, the main idea of HFS-FEM is to establish an appropriate hybrid FE formulation whereby intra-element continuity is enforced on a nonconforming intra-element field formed by a linear combination of fundamental solutions at points outside the element domain under consideration, while an auxiliary frame field is independently defined on the element boundary to enforce the field continuity across inter-element boundaries. But unlike in the HT FEM, the intra-element fields are constructed based on the fundamental solution, rather than T-functions. Consequently, a variational functional corresponding to the new trial function is required to derive the related stiffness matrix equation. As was done in conventional FEM, the solution domain is divided into sub-domains or elements. For a particular element, say element *e*, its domain is denoted by Ω_e and bounded by Γ_e. Since a nonconforming function is used for modeling intra-element field, additional continuities are usually required over the common boundary Γ_{Ief} between any two adjacent elements '*e*' and '*f*' (see Figure 8)[39]:

$$\left.\begin{array}{l}\Psi_e=\Psi_f\ \ \text{(conformity)}\\ p_e+p_f=0\ \ \text{(reciprocity)}\end{array}\right\}\ \text{on}\ \ \Gamma_{Ief}=\Gamma_e\cap\Gamma_f \qquad (81)$$

in the proposed hybrid FE approach.

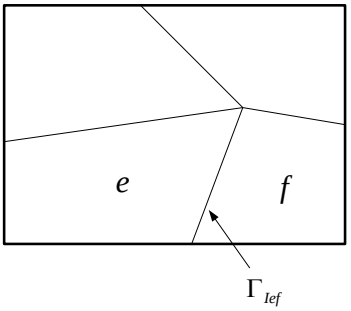

Figure 8 Illustration of continuity between two adjacent elements 'e' and 'f'

IV.3.1 Non-conforming intra-element field

For a particular element, say element *e*, which occupies sub-domain Ω_e, the field variable within the element is extracted from a linear combination of fundamental solutions centered at different source points (see 错误!未找到引用源。 5), that

$$\Psi_e(\mathbf{x})=\sum_{j=1}^{n_s}N_e(\mathbf{x},\mathbf{y}_j)c_{ej}=\mathbf{N}_e(\mathbf{x})\mathbf{c}_e\ \ \forall\mathbf{x}\in\Omega_e,\mathbf{y}_j\notin\Omega_e \qquad (82)$$

where c_{ej} is undetermined coefficients and n_s is the number of virtual sources outside the element *e*. $N_e(\mathbf{x},\mathbf{y}_j)$ is the required fundamental solution expressed in terms of local element coordinates (x_1,x_2), instead of global coordinates (X_1,X_2) (see Fig.5). Obviously, Eq (51) analytically satisfies the heat conduction equation (75) due to the inherent property of $N_e(\mathbf{x},\mathbf{y}_j)$.

The fundamental solution for FGM (N_e in Eq.(51)) is used to approximate the intra-element field in FGM. It is well known that the fundamental solution represents the filed generated by a concentrated unit source acting at a point, so the smooth variation of material properties throughout an element can be achieved by this inherent property, instead of the stepwise constant approximation, which has been frequently used in the conventional FEM. For example, 错误!未找到引用源。9 illustrates the difference between the two models when the thermal conductivity varies along direction X_2 in isotropic material.

Note that the thermal conductivity in Eq. (74) is defined in the global coordinate system. When

contriving the intra-element field for each element, this formulation has to be transferred into local element coordinate system defined at the center of the element, the graded matrix $\mathbf{K}^*$ in Eq. (74) can, then, be expressed by

$$\mathbf{K}_e^*(\mathbf{x}) = \mathbf{K}_C \exp(2\boldsymbol{\beta}\cdot\mathbf{x}) \tag{83}$$

for a particular element *e*, where $\mathbf{K}_\mathbf{C}$ denotes the value of conductivity at the centroid of each element and can be calculated as follows:

$$\mathbf{K}_C = \mathbf{K}\exp(2\boldsymbol{\beta}\cdot\mathbf{X}_c) \tag{84}$$

where $\mathbf{X}_c$ is the global coordinates of the element centroid.

Accordingly, the matrix $\mathbf{K}_C$ is used to replace **K** (see Eq.(77)) in the formulation of fundamental solution for FGM and to construct intra-element field in the coordinate system local to element.

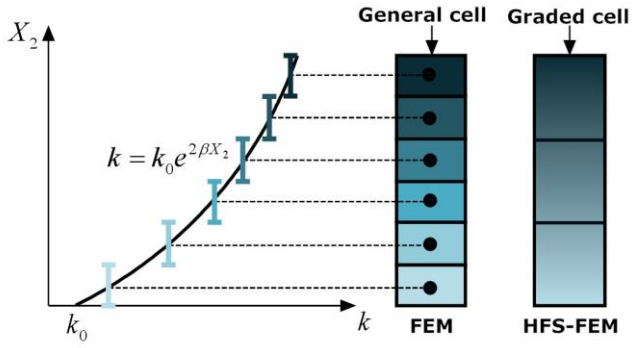

Figure 9 Comparison of computational cell in the conventional FEM and the proposed HFS-FEM

In practice, the generation of virtual sources is usually done by means of the following formulation employed in the MFS [70]

$$\mathbf{y} = \mathbf{x}_b + \mu\left(\mathbf{x}_b - \mathbf{x}_c\right) \tag{85}$$

where μ is a dimensionless coefficient (μ=2.5 in our analysis [7]), $\mathbf{x}_b$ and $\mathbf{x}_c$ are, respectively, boundary point and geometrical centroid of the element. For a particular element shown in Fig. 5, we can use the nodes of element to generate related source points.

The corresponding normal heat flux on Γ_e is given by

$$p_e = -\mathbf{K}_e^* \frac{\partial \Psi_e}{\partial X_j} n_i = \mathbf{Q}_e \mathbf{c}_e \tag{86}$$

where

$$\mathbf{Q}_e = -\mathbf{K}_e^* \frac{\partial \mathbf{N}_e}{\partial X_j} n_i = -\mathbf{A}\mathbf{K}_e^* \mathbf{T}_e \tag{87}$$

with

$$\mathbf{T}_e = \begin{bmatrix} \mathbf{N}_{e,1} & \mathbf{N}_{e,2} \end{bmatrix}^{\mathrm{T}} \qquad \mathbf{A} = \begin{bmatrix} n_1 & n_2 \end{bmatrix} \tag{88}$$

IV.3.2 Auxiliary conforming frame field

In order to enforce the conformity on the field variable u, for instance, $\Psi_e = \Psi_f$ on $\Gamma_e \cap \Gamma_f$ of any two neighboring elements *e* and *f*, an auxiliary inter-element frame field $\tilde{\Psi}$ is used and expressed in terms of nodal degrees of freedom (DOF), $\mathbf{d}$, as used in the conventional finite elements as

$$\tilde{\Psi}_e(\mathbf{x}) = \tilde{\mathbf{N}}_e(\mathbf{x})\mathbf{d}_e \tag{89}$$

which is independently assumed along the element boundary, where $\tilde{\mathbf{N}}_e$ represents the conventional FE interpolating functions. For example, a simple interpolation of the frame field on the side with three nodes of a particular element can be given in the form

$$\tilde{\Psi} = \tilde{N}_1\Psi_1 + \tilde{N}_2\Psi_2 + \tilde{N}_3\Psi_3 \tag{90}$$

where $\tilde{N}_i$ ($i = 1,2,3$) stands for shape functions in terms of natural coordinate ξ defined in 错误!未找到引用源。6.

IV.4 Modified variational principle and stiffness equation

IV.4.1 Modified variational functional

For the boundary value problem defined in Eqs.(73) and (79)-(80), since the stationary conditions of the traditional potential or complementary variational functional can't guarantee the satisfaction of inter-element continuity condition required in the proposed HFS-FE model, a modified potential functional is developed as follows [7]

$$\begin{aligned}\Pi_m = \sum_e \Pi_{me} = \sum_e [&- \int_{\Omega_e} \frac{1}{2} K_{ij}^* \Psi_{,i} \Psi_{,j} \mathrm{d}\Omega \\ &- \int_{\Gamma_{qe}} \bar{q}\tilde{\Psi}\mathrm{d}\Gamma + \int_{\Gamma_e} \left(\tilde{\Psi} - \Psi\right) p \mathrm{d}\Gamma]\end{aligned} \tag{91}$$

in which the governing equation (73) is assumed to be satisfied, a *priori*, in deriving the HFS-FE model (For convenience, the repeated subscript indices stand for summation convention). The boundary Γ_e of a particular element consists of the following parts

$$\Gamma_e = \Gamma_{ue} \cup \Gamma_{qe} \cup \Gamma_{Ie} \tag{92}$$

where Γ_{Ie} represents the inter-element boundary of the element '*e*' shown in Fig. 1.

The stationary condition of the functional (59) can lead to the governing equation (Euler equation), boundary

conditions and continuity conditions, details of the derivation can refer to Ref. [7].

IV.4.2 Stiffness equation

Having independently defined the intra-element field and frame field in a particular element (see Fig. 2), the next step is to generate the element stiffness equation through a variational approach and to establish a linkage between the two independent fields.

The variational functional Π_e corresponding to a particular element e of the present problem can be written as

$$\begin{aligned}\Pi_{me} = &-\frac{1}{2}\int_{\Omega_e} K_{ij}^{*}\Psi_{,i}\Psi_{,j}\mathrm{d}\Omega \\ &-\int_{\Gamma_{qe}} \bar{q}\tilde{\Psi}\mathrm{d}\Gamma+\int_{\Gamma_e} p\left(\tilde{\Psi}-\Psi\right)\mathrm{d}\Gamma\end{aligned} \tag{93}$$

Appling the Gauss theorem to the above functional, we have the following functional for the HFS-FE model

$$\begin{aligned}\Pi_{me} = &\frac{1}{2}\left[\int_{\Gamma_e} p\Psi\mathrm{d}\Gamma+\int_{\Omega_e}\Psi(K_{ij}^{*}u_{,i})_{,j}\mathrm{d}\Omega\right] \\ &-\int_{\Gamma_{qe}} \bar{q}\tilde{\Psi}\mathrm{d}\Gamma+\int_{\Gamma_e} p\left(\tilde{\Psi}-\Psi\right)\mathrm{d}\Gamma\end{aligned} \tag{94}$$

Considering the governing equation (73), we finally have the functional defined on the element boundary only

$$\Pi_{me} = -\frac{1}{2}\int_{\Gamma_e} p\Psi\mathrm{d}\Gamma-\int_{\Gamma_{qe}} \bar{q}\tilde{\Psi}\mathrm{d}\Gamma+\int_{\Gamma_e} p\tilde{\Psi}\mathrm{d}\Gamma \tag{95}$$

which yields by substituting Eqs (51), (54) and (57) into the functional (95)

$$\Pi_e = -\frac{1}{2}\mathbf{c}_e^{\mathrm{T}}\mathbf{H}_e\mathbf{c}_e-\mathbf{d}_e^{\mathrm{T}}\mathbf{g}_e+\mathbf{c}_e^{\mathrm{T}}\mathbf{G}_e\mathbf{d}_e \tag{96}$$

with

$$\mathbf{H}_e=\int_{\Gamma_e}\mathbf{Q}_e^{\mathrm{T}}\mathbf{N}_e\mathrm{d}\Gamma,\ \mathbf{G}_e=\int_{\Gamma_e}\mathbf{Q}_e^{\mathrm{T}}\tilde{\mathbf{N}}_e\mathrm{d}\Gamma,\ \mathbf{g}_e=\int_{\Gamma_{qe}}\tilde{\mathbf{N}}_e^{\mathrm{T}}\bar{\mathrm{q}}\mathrm{d}\Gamma \tag{97}$$

V.F-Trefftz method for skin burn problems

V.1 Skin tissue under laser heating

The two-dimensional skin model used in [76] is chosen here, in which the skin material is assumed to be homogeneous and isotropic. In the model displayed in Fig. 10, the outer surface of the skin tissue is subjected to the convention condition and the inner boundary is distant from the skin surface, where the temperature remains at the constant core temperature. The upper and lower surfaces are treated as adiabatic by assuming that tissue remote from the area of interest is not affected by the imposed thermal disturbance. A Gaussian type laser beam is introduced as the internal spatial heat source and the Beer-Lambert law is used to model the exponential decay of heat generation by laser heating inside the tissue.

Due to the symmetry of the skin model, only half of the model is taken into consideration in the analysis, say the upper half shaded region displayed in Fig. 10 in which x denotes the tissue depth from the skin surface, y is the distance along the skin surface, and a rectangular domain of 4cm length and 3cm width is employed as the solution domain [76]. The thermal properties of skin tissues used in the analysis are listed in Table 1 [77].

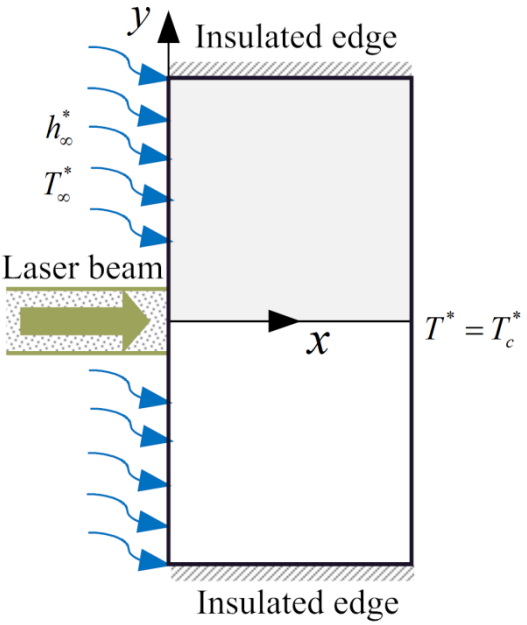

Figure 10 Simplified skin model of two-dimensional skin tissue

Table 1 Thermal properties of skin tissue

Thermal properties of skin	*Value*
Thermal conductivity k ($\mathrm{Wm^{-1}K^{-1}}$)	0.5
Density ρ ($\mathrm{kgm^{-3}}$)	1000
Specific heat c ($\mathrm{Jkg^{-1}K^{-1}}$)	4200
Blood perfusion rate ω_b ($\mathrm{m^3s^{-1}m^{-3}}$)	0.0005
Density of blood ρ_b ($\mathrm{kgm^{-3}}$)	1000
Specific heat of blood c_b ($\mathrm{Jkg^{-1}K^{-1}}$)	4200
Metabolic heat Q_m ($\mathrm{Wm^{-3}}$)	4200

As shown in Fig. 10, the laser beam, assumed to be produced from a CO_2 laser with scanner head and beam expander, injects directly onto the middle point (0, 0) of the skin surface. In the present work, the pattern of the

laser beam is that of Gaussian distribution with 2.85mm standard deviation [78]. The Beer-Lambert law is used to model the laser heat absorption in the two dimensional skin model, and thus the spatial heat source Q_r caused by laser heating is described by

$$Q_r^*(x,y,t) = P_{in}\mu_a e^{(-\mu_a x)} \frac{1}{\sigma\sqrt{2\pi}} e^{\left(\frac{-y^2}{2\sigma^2}\right)} \quad (98)$$

where P_{in} represents the laser power setting, μ_a the absorption coefficient of the skin tissue determined by the wave length of the laser, and σ is the standard deviation of the laser beam profile.

V.2 General mathematical equations

Referring to the Cartesian coordinate system shown in Fig. 10, the bioheat transfer in a biological tissue is adequately described by the well-known Pennes equation in the following general form:

$$k^*\nabla^2 T^* + \rho_b^* c_b^* \omega_b^* \left(T_a^* - T^*\right) + Q_t^* = \rho^* c^* \frac{\partial T^*}{\partial t^*} \quad (99)$$

with the boundary conditions

$$\begin{cases} T^*(\mathbf{x},t^*) = \overline{T}^*(\mathbf{x},t^*) & \mathbf{x}\in\Gamma_1 \\ q^*(\mathbf{x},t^*) = \overline{q}^*(\mathbf{x},t^*) & \mathbf{x}\in\Gamma_2 \\ q^*(\mathbf{x},t^*) = h_\infty^*(T^* - T_\infty^*) & \mathbf{x}\in\Gamma_3 \end{cases} \quad (100)$$

where ∇^2 represents the Laplacian operator, $T^*(\mathbf{x},t^*)$ is the sought temperature field variable, t^* denotes time ($t^* > 0$). k^* is the thermal conductivity dependent on the special variables $\mathbf{x}\in\Omega$; ρ^* is the mass density and c is the specific heat. $Q_t^* = Q_m^* + Q_r^*$ stands for the general internal heat generation per unit volume due to metabolic heat and the laser beam. q^* represents the boundary normal heat flux defined by

$$q^* = -k^*\nabla T^*\cdot\mathbf{n} = -k^*\frac{\partial T^*}{\partial n} \quad (101)$$

n is the unit outward normal to the boundary Γ. A variable with over-bar denotes the variable being specified on given boundary. The constant T_a^* is artery temperature. The constant h_∞^* is the convection coefficient and T_∞^* is the environmental temperature. For a well-posed problem, we have $\Gamma = \Gamma_1 \cup \Gamma_2 \cup \Gamma_3$.

Finally, the initial condition is defined as

$$T^*(\mathbf{x},t^*=0) = T_0^*(x) \quad (102)$$

To avoid the potential numerical overflow of the present algorithm, the following dimensionless variables are employed in the analysis [79]:

$$\begin{aligned} &X = \frac{x}{L_0},\ Y = \frac{y}{L_0},\ T = \frac{\left(T^* - T_a^*\right)k_0}{Q_0 L_0^2},\ k = \frac{k^*}{k_0} \\ &\rho = \frac{\rho^*}{\rho_0},\ c = \frac{c^*}{c_0},\ t = \frac{t^* k_0}{L_0^2\rho_0 c_0},\ Q_t = \frac{Q_t^*}{Q_0} \end{aligned} \quad (103)$$

where L_0 is the reference length of the biological body, k_0, ρ_0, c_0, and Q_0 are respectively reference values of the thermal conductivity, density, specific heat of tissue, and heat source term.

From Eq. (103) we derive

$$\begin{aligned} &\frac{\partial T^*}{\partial x} = \frac{Q_0 L_0^2}{k_0}\frac{1}{L_0}\frac{\partial T}{\partial X},\quad \frac{\partial T^*}{\partial y} = \frac{Q_0 L_0^2}{k_0}\frac{1}{L_0}\frac{\partial T}{\partial Y} \\ &\frac{\partial^2 T^*}{\partial x^2} = \frac{Q_0 L_0^2}{k_0}\frac{1}{L_0^2}\frac{\partial^2 T}{\partial X^2},\ \frac{\partial^2 T^*}{\partial y^2} = \frac{Q_0 L_0^2}{k_0}\frac{1}{L_0^2}\frac{\partial^2 T}{\partial Y^2} \\ &\frac{\partial T^*}{\partial t^*} = \frac{Q_0 L_0^2}{k_0}\frac{k_0}{L_0^2\rho_0 c_0}\frac{\partial T}{\partial t}, \end{aligned} \quad (104)$$

Substitution of Eq. (102) and Eq. (104) into Eq. (99) yields

$$k\nabla^2 T(\mathbf{x},t) - \rho_b c_b \omega_b T(\mathbf{x},t) + Q_t(\mathbf{x}) = \rho c\frac{\partial T(\mathbf{x},t)}{\partial t} \quad (105)$$

where

$$\rho_b c_b \omega_b = \frac{\rho_b^* c_b^* \omega_b^* L_0^2}{k_0} \quad (106)$$

Correspondingly, the boundary conditions are rewritten as

$$\begin{cases} T(\mathbf{x},t) = \overline{T}(\mathbf{x},t) & \mathbf{x}\in\Gamma_1 \\ q(\mathbf{x},t) = \overline{q}(\mathbf{x},t) & \mathbf{x}\in\Gamma_2 \\ q(\mathbf{x},t) = h_\infty(T - T_\infty) & \mathbf{x}\in\Gamma_3 \end{cases} \quad (107)$$

with

$$\begin{aligned} &\overline{T} = \frac{\left(\overline{T}^* - T_a^*\right)k_0}{Q_0 L_0^2},\ \overline{q} = \frac{\overline{q}^*}{Q_0 L_0}, \\ &h_\infty = \frac{h_\infty^* L_0}{k_0},\ T_\infty = \frac{\left(T_\infty^* - T_a^*\right)k_0}{Q_0 L_0^2} \end{aligned} \quad (108)$$

and

$$q = -k\frac{\partial T}{\partial n} \quad (109)$$

V.3 Transient T-Trefftz FEM formulation

V.3.1 Direct time stepping

Making use of finite difference method, the derivative of temperature can be written as

$$\frac{\partial T(\mathbf{x},t)}{\partial t}=\frac{T^{n+1}(\mathbf{x})-T^{n}(\mathbf{x})}{\Delta t} \tag{110}$$

where Δt is the time-step, $T^{n+1}(\mathbf{x})=T(\mathbf{x},t^{n+1})$ and $T^{n}(\mathbf{x})=T(\mathbf{x},t^{n})$ represent the temperature at the time instances t^{n+1} and t^{n}, respectively.

As a result, Eq. (105) at the time instance t^{n+1} can be rewritten as

$$\begin{aligned} &k\nabla^2 T^{n+1}(\mathbf{x})-\rho_b c_b \omega_b T^{n+1}(\mathbf{x})+Q_t(\mathbf{x}) \\ &\quad=\rho c\frac{T^{n+1}(\mathbf{x})-T^{n}(\mathbf{x})}{\Delta t} \end{aligned} \tag{111}$$

Rearranging Eq. (111) gives

$$\nabla^2 T^{n+1}(\mathbf{x})-\lambda^2 T^{n+1}(\mathbf{x})=b(\mathbf{x}) \tag{112}$$

with

$$\lambda=\sqrt{\frac{\rho c}{k\Delta t}+\frac{\rho_b c_b \omega_b}{k}} \tag{113}$$

and

$$b(\mathbf{x})=-\frac{1}{k}Q_t(\mathbf{x})-\frac{\rho c}{k\Delta t}T^{n}(\mathbf{x}) \tag{114}$$

Accordingly, the boundary conditions at time instance t^{n+1} can be represented as

$$\begin{cases} T^{n+1}(\mathbf{x})=\overline{T}(\mathbf{x},t^{n+1}) & \mathbf{x}\in\Gamma_1 \\ q^{n+1}(\mathbf{x})=\overline{q}(\mathbf{x},t^{n+1}) & \mathbf{x}\in\Gamma_2 \\ q^{n+1}(\mathbf{x})=h_\infty(T^{n+1}-T_\infty) & \mathbf{x}\in\Gamma_3 \end{cases} \tag{115}$$

The linear system consisting of the governing partial differential equation (112) and boundary conditions (115) is a standard inhomogeneous modified Helmholtz system, which will be solved by means of the present HFS-FEM and the dual reciprocity technique based on radial basis function interpolation described in the following sections.

V.3.2 Particular solution obtained using radial basis functions

Let T_p^{n+1} be a particular solution of the governing equation (112), we have

$$\nabla^2 T_p^{n+1}(\mathbf{x})-\lambda^2 T_p^{n+1}(\mathbf{x})=b(\mathbf{x}) \tag{116}$$

but does not necessarily satisfy boundary condition (115).

Subsequently, the system consisting of Eq. (112) and Eq. (115) can be reduced to a homogeneous system by introducing two new variables as follows:

$$\begin{aligned} T_h^{n+1}(\mathbf{x})&=T^{n+1}(\mathbf{x})-T_p^{n+1}(\mathbf{x}) \\ q_h^{n+1}(\mathbf{x})&=q^{n+1}(\mathbf{x})-q_p^{n+1}(\mathbf{x}) \end{aligned} \tag{117}$$

where

$$q_h^{n+1}(\mathbf{x})=-k\frac{\partial T_h^{n+1}(\mathbf{x})}{\partial n},\qquad q_p^{n+1}(\mathbf{x})=-k\frac{\partial T_p^{n+1}(\mathbf{x})}{\partial n} \tag{118}$$

Substituting Eq. (117) into Eq. (112), we obtain the following homogeneous equation

$$\nabla^2 T_h^{n+1}(\mathbf{x})-\lambda^2 T_h^{n+1}(\mathbf{x})=0 \tag{119}$$

with modified boundary conditions

$$\begin{cases} T_h^{n+1}(\mathbf{x})=\overline{T}_h(\mathbf{x})=\overline{T}(\mathbf{x},t^{n+1})-T_p^{n+1}(\mathbf{x}) & \mathbf{x}\in\Gamma_1 \\ q_h^{n+1}(\mathbf{x})=\overline{q}_h(\mathbf{x})=\overline{q}(\mathbf{x},t^{n+1})-q_p^{n+1}(\mathbf{x}) & \mathbf{x}\in\Gamma_2 \\ q_h^{n+1}(\mathbf{x})=h_\infty\left\{T_h^{n+1}(\mathbf{x})-T_\infty^{n+1}(\mathbf{x})\right\} & \mathbf{x}\in\Gamma_3 \end{cases} \tag{120}$$

where

$$T_\infty^{n+1}(\mathbf{x})=-T_p^{n+1}(\mathbf{x})+T_\infty+\frac{q_p^{n+1}(\mathbf{x})}{h_\infty}$$

The above homogeneous system can be solved using the hybrid finite element model described in the next section.

In what follows, we describe the solution procedure for the particular solution part $T_p^{n+1}(\mathbf{x})$. For the arbitrary right-handed source term $b(\mathbf{x})$, the particular solution $T_p^{n+1}(\mathbf{x})$ can be determined numerically by the dual reciprocity technique, in which it is essential to approximate the source term by a series of basis functions, i.e. radial basis functions (RBFs).

Let ϕ be a radial basis function. Then the source term $b(\mathbf{x})$ in Eq. (116) can be approximated as follows [14, 80]:

$$b(\mathbf{x})=\sum_{j=1}^{M}\alpha_j\phi(r_j) \tag{121}$$

where $r_j=\left\|\mathbf{x}-\mathbf{x}_j\right\|$ denotes the Euclidean distance between the field point $\mathbf{x}$ and source point $\mathbf{x}_j$, and α_j are unknown coefficients.

Making use of Eq. (121), the particular solution can be obtained as

$$T_p^{n+1}(\mathbf{x})=\sum_{j=1}^{M}\alpha_j\Phi(r_j) \tag{122}$$

where the function is governed by

$$\nabla^2\Phi(r_j)-\lambda^2\Phi(r_j)=\phi(r_j) \tag{123}$$

Taking the thin plate spline (TPS)

$$\phi(r_j) = r_j^2 \ln(r_j) \tag{124}$$

as an example, the approximate particular solution $\Phi(r_j)$ can be obtained by the annihilator method as [81]

$$\Phi(r_j) = \begin{cases} -\dfrac{4}{\lambda^4} - \dfrac{4}{\lambda^4}\ln r_j - \dfrac{1}{\lambda^2} r_j^2 \ln r_j \\ \qquad -\dfrac{4}{\lambda^4} K_0\left(\lambda r_j\right), \quad r_j \neq 0 \\ -\dfrac{4}{\lambda^4} + \dfrac{4\gamma}{\lambda^4} + \dfrac{4}{\lambda^4}\ln\left(\dfrac{\lambda}{2}\right), \quad r_j = 0 \end{cases} \tag{125}$$

where γ =0.5772156649015328 is Euler's constant.

V.3.3 Homogeneous solution using the hybrid finite element model

To perform the hybrid finite element analysis in a convenient way, the boundary conditions given in Eq. (120) are rewritten as

$$\begin{cases} T_h^{n+1}(\mathbf{x}) = \overline{T}_h(\mathbf{x}) & \mathbf{x} \in \Gamma_1 \\ \chi_h^{n+1}(\mathbf{x}) = \overline{\chi}_h(\mathbf{x}) & \mathbf{x} \in \Gamma_2 \\ \chi_h^{n+1}(\mathbf{x}) = \overline{h}_\infty \left\{ T_h^{n+1}(\mathbf{x}) - T_\infty^{n+1}(\mathbf{x}) \right\} & \mathbf{x} \in \Gamma_3 \end{cases} \tag{126}$$

with

$$\chi_h^{n+1}(\mathbf{x}) = \frac{\partial T_h^{n+1}(\mathbf{x})}{\partial n},\ \overline{\chi}_h(\mathbf{x}) = -\overline{q}_h(\mathbf{x})/k,\ \overline{h}_\infty = -\frac{h_\infty}{k} \tag{127}$$

Then, the following hybrid variational functional expressed at element level can be constructed as [14]

$$\begin{aligned} \Pi_{me} = {} & \frac{1}{2}\int_{\Omega_e} \left(T_{,i} T_{,i} + \lambda^2 T^2 \right) \mathrm{d}\Omega - \int_{\Gamma_{2e}} \overline{\chi}\tilde{T}\,\mathrm{d}\Gamma \\ & + \int_{\Gamma_e} \chi\left(\tilde{T} - T\right)\mathrm{d}\Gamma - \frac{1}{2}\int_{\Gamma_{3e}} \overline{h}_\infty \left(\tilde{T} - T_\infty\right)^2 \mathrm{d}\Gamma \end{aligned} \tag{128}$$

in which T is the temperature field defined inside the element domain Ω_e with the boundary Γ_e, $\tilde{T}$ denotes the frame field defined along the element boundary, and $\Gamma_{2e} = \Gamma_2 \cap \Gamma_e$, $\Gamma_{3e} = \Gamma_3 \cap \Gamma_e$. Note that in Eq. (128), the superscript '*n*+1' and subscript '*h*' are discarded for the sake of simplicity.

By invoking the divergence theorem and assuming that $\tilde{T}$ satisfies the specified temperature boundary condition (the first equation of Eq. (126)) and the compatibility condition on the interface between the element under consideration and its adjacent elements as prerequisites, variation of Eq. (128) can be written as

$$\begin{aligned} \delta\Pi_{me} = {} & -\int_{\Omega_e} \left(T_{,ii} - \lambda^2 T \right) \delta T \mathrm{d}\Omega \\ & + \int_{\Gamma_{2e}} \left(\chi - \overline{\chi} \right) \delta\tilde{T}\mathrm{d}\Gamma + \int_{\Gamma_e} \delta\chi \left(\tilde{T} - T \right)\mathrm{d}\Gamma \\ & + \int_{\Gamma_{3e}} \left[\chi - \overline{h}_\infty \left(\tilde{T} - T_\infty \right) \right] \delta\tilde{T}\mathrm{d}\Gamma \end{aligned} \tag{129}$$

from which it can be seen that the third integral enforces the equality of T and $\tilde{T}$ along the element boundary Γ_e. The first, second and fourth integrals enforce respectively the governing equation (119), flux, and convection boundary conditions (the second and third equations in (126)).

If the internal temperature field T satisfies the homogeneous modified Helmholtz equation, i.e.

$$\nabla^2 T - \lambda^2 T = 0 \tag{130}$$

pointwise, then applying the divergence theorem again to the functional (128), we have

$$\begin{aligned} \Pi_{me} = {} & -\frac{1}{2}\int_{\Gamma_e} \chi T \mathrm{d}\Gamma - \int_{\Gamma_{2e}} \overline{\chi}\tilde{T}\mathrm{d}\Gamma \\ & + \int_{\Gamma_e} \chi\tilde{T}\mathrm{d}\Gamma - \int_{\Gamma_{3e}} \frac{\overline{h}_\infty}{2}\left(\tilde{T} - T_\infty\right)^2 \mathrm{d}\Gamma \end{aligned} \tag{131}$$

which involves boundary integrals only.

In the proposed HFS-FEM, the variable T is given as a superposition of fundamental solutions $G^*(P, Q_j)$ at n_s source points to guarantee the satisfaction of Eq. (130)

$$T_h^{n+1} = \sum_{j=1}^{n_s} G^*(P, Q_j) c_{ej} = \mathbf{N}_e(P)\mathbf{c}_e, \quad P \in \Omega_e, Q_j \notin \Omega_e \tag{132}$$

where c_{ej} is undetermined coefficients and n_s is the number of virtual sources Q_j applied at points outside the element.

The free-space fundamental solution of the modified Helmholtz operator can be obtained as the solution of

$$\nabla^2 G^*(P, Q_j) - \lambda^2 G^*(P, Q_j) = -\delta(P, Q_j) \tag{133}$$

and is given by [82]

$$G^*(P, Q_j) = -\frac{1}{2\pi} K_0(\lambda \left\| P - Q_j \right\|) \tag{134}$$

where $\delta(P, Q_j)$ is the Dirac delta function and K_0 denotes the modified Bessel function of the second kind with order 0.

Simultaneously, the independent frame variable on the element boundary can be defined by the standard shape function interpolation

$$\tilde{T}(P)=\sum_{i=1}^{n}\tilde{N}_i(P)d_{ei}=\tilde{\mathbf{N}}_e(P)\mathbf{d}_e,\quad P\in\Gamma_e \quad (135)$$

where n is the number of nodes of the element under consideration, $\tilde{N}_i$ is the shape function and d_{ei} is nodal temperature. Their descriptions can be found in standard finite element texts and are not repeated here.

By substitution of Eq. (132) and Eq. (135) into Eq. (131) we obtain

$$\begin{aligned}\Pi_{me}=&-\frac{1}{2}\mathbf{c}_e^{\mathrm{T}}\mathbf{H}_e\mathbf{c}_e-\mathbf{d}_e^{\mathrm{T}}\mathbf{g}_e+\mathbf{c}_e^{\mathrm{T}}\mathbf{G}_e\mathbf{d}_e\\&-\frac{1}{2}\mathbf{d}_e^{\mathrm{T}}\mathbf{F}_e\mathbf{d}_e+\mathbf{d}_e^{\mathrm{T}}\mathbf{f}_e-\mathbf{a}_e\end{aligned} \quad (136)$$

in which

$$\begin{aligned}&\mathbf{H}_e=\int_{\Gamma_e}\mathbf{Q}_e^{\mathrm{T}}\mathbf{N}_e\mathrm{d}\Gamma,\quad \mathbf{G}_e=\int_{\Gamma_e}\mathbf{Q}_e^{\mathrm{T}}\tilde{\mathbf{N}}_e\mathrm{d}\Gamma,\\&\mathbf{g}_e=\int_{\Gamma_{2e}}\tilde{\mathbf{N}}_e^{\mathrm{T}}\bar{q}\mathrm{d}\Gamma,\quad \mathbf{F}_e=\int_{\Gamma_{3e}}\bar{h}_\infty\tilde{\mathbf{N}}_e^{\mathrm{T}}\tilde{\mathbf{N}}_e\mathrm{d}\Gamma,\\&\mathbf{f}_e=\int_{\Gamma_{3e}}\bar{h}_\infty T_\infty\tilde{\mathbf{N}}_e^{\mathrm{T}}\mathrm{d}\Gamma,\ \mathbf{a}_e=\int_{\Gamma_{3e}}\frac{\bar{h}_\infty T_\infty^2}{2}\mathrm{d}\Gamma\end{aligned} \quad (137)$$

and

$$\mathbf{Q}_e=\frac{\partial\mathbf{N}_e}{\partial n} \quad (138)$$

VI.Conclusions and future developments

On the basis of the preceding discussion, the following conclusions can be drawn. In contrast to conventional FE and boundary element models, the main advantages of the Trefftz model are: (a) the formulation calls for integration along the element boundaries only, which enables arbitrary polygonal or even curve-sided elements to be generated; (b) the Trefftz FE model is likely to represent the optimal expansion bases for hybrid-type elements where inter-element continuity need not be satisfied, a priori, which is particularly important for generating a quasi-conforming plate bending element; (c) the model offers the attractive possibility of developing accurate functionally graded elements.

It is recognized that the Trefftz FEM has become increasingly popular as an efficient numerical tool in computational mechanics since their initiation in the late seventies. However, there are still many possible extensions and areas in need of further development in the future. Among those developments one could list the following:

1 Development of efficient Trefftz FE-BEM schemes for complex engineering structures and the related general purpose computer codes with preprocessing and postprocessing capabilities.

2 Generation of various special-purpose elements to effectively handle singularities attributable to local geometrical or load effects (holes, cracks, inclusions, interface, corner and load singularities). The special-purpose functions warrant that excellent results are obtained at minimal computational cost and without local mesh refinement. 3 Development of HT FE in conjunction with a topology optimization scheme to contribute to microstructure design.

3 Extension of the Trefftz-FEM to elastodynamics, fluid flow, dynamics of thin and thick plate bending and fracture mechanics, soil mechanics, deep shell structure, and rheology problems.

4 Development of multiscale framework across from continuum to micro- and nano-scales for modeling heterogeneous and functional materials.

REFERENCES

[1] H.C. Martin, G.F. Carey, Introduction to Finite Element Analysis: Theory and Applications, McGraw-Hill Book Company, New York 1973.

[2] J.H. Argyris, M. Kleiber, Incremental formulation in nonlinear mechanics and large strain elasto-plasticity - natural approach .1, Computer Methods in Applied Mechanics and Engineering, 11 (1977) 215-247.

[3] J.H. Argyris, J.S. Doltsinis, M. Kleiber, Incremental formulation in non-linear mechanics and large strain elasto-plasticity - Natural approach .2, Computer Methods in Applied Mechanics and Engineering, 14 (1978) 259-294.

[4] J. Jirousek, N. Leon, Powerful finite-element for plate bending, Computer Methods in Applied Mechanics and Engineering, 12 (1977) 77-96.

[5] Q.H. Qin, C.X. Mao, Coupled torsional-flexural vibration of shaft systems in mechanical engineering .I. Finite element model, Computers & Structures, 58 (1996) 835-843.

[6] Q.H. Qin, The Trefftz finite and boundary element method, WIT Press, Southampton, 2000.

[7] H. Wang, Q.H. Qin, Hybrid FEM with fundamental solutions as trial functions for heat conduction simulation, Acta Mechanica Solida Sinica, 22 (2009) 487-498.

[8] J.H. Argyris, P.C. Dunne, M. Haase, J. Orkisz, Higher-order simplex elements for large strain analysis - Natural approach, Computer Methods in Applied Mechanics and Engineering, 16 (1978) 369-403.

[9] C.X. Mao, Q.H. Qin, Coupled torsional-flexural vibration of shaft systems in mechanical engineering—II. FE-TM impedance coupling method, Computers & Structures, 58 (1996) 845-849.

[10] Q.H. Qin, Y. Mai, BEM for crack-hole problems in thermopiezoelectric materials, Engineering Fracture Mechanics, 69 (2002) 577-588.

[11] C. Cao, A. Yu, Q.H. Qin, Evaluation of effective thermal conductivity of fiber-reinforced composites by boundary integral based finite element method, International Journal of Architecture, Engineering and Construction, 1 (2012) 14-29.
[12] L. Cao, H. Wang, Q.H. Qin, Fundamental solution based graded element model for steady-state heat transfer in FGM, Acta Mechanica Solida Sinica, 25 (2012) 377-392.
[13] J. Jirousek, Basis for development of large finite-elements locally satisfying all field equations, Computer Methods in Applied Mechanics and Engineering, 14 (1978) 65-92.
[14] Q.H. Qin, H. Wang, Matlab and C programming for Trefftz finite element methods, New York: CRC Press, 2008.
[15] Q.H. Qin, Trefftz finite element method and its applications, Applied Mechanics Reviews, 58 (2005) 316-337.
[16] W. Chen, Z.-J. Fu, Q.H. Qin, Boundary particle method with high-order Trefftz functions, Computers, Materials & Continua (CMC), 13 (2010) 201-217.
[17] H. Wang, Q.H. Qin, D. Arounsavat, Application of hybrid Trefftz finite element method to non‐linear problems of minimal surface, International Journal for Numerical Methods in Engineering, 69 (2007) 1262-1277.
[18] H. Wang, Q.H. Qin, X.P. Liang, Solving the nonlinear Poisson-type problems with F-Trefftz hybrid finite element model, Engineering Analysis with Boundary Elements, 36 (2012) 39-46.
[19] Q.H. Qin, Dual variational formulation for Trefftz finite element method of elastic materials, Mechanics Research Communications, 31 (2004) 321-330.
[20] Q.H. Qin, Formulation of hybrid Trefftz finite element method for elastoplasticity, Applied mathematical modelling, 29 (2005) 235-252.
[21] Q.H. Qin, Trefftz plane elements of elastoplasticity with p-extension capabilities, Journal of Mechanical Engineering, 56 (2005) 40-59.
[22] Y. Cui, Q.H. Qin, J.-S. WANG, Application of HT finite element method to multiple crack problems of Mode I, II and III, Chinese Journal of Engineering Mechanics, 23 (2006) 104-110.
[23] Y. Cui, J. Wang, M. Dhanasekar, Q.H. Qin, Mode III fracture analysis by Trefftz boundary element method, Acta Mechanica Sinica, 23 (2007) 173-181.
[24] C. Cao, Q.H. Qin, A. Yu, Micromechanical Analysis of Heterogeneous Composites using Hybrid Trefftz FEM and Hybrid Fundamental Solution Based FEM, Journal of Mechanics, 29 (2013) 661-674.
[25] M. Dhanasekar, J. Han, Q.H. Qin, A hybrid-Trefftz element containing an elliptic hole, Finite Elements in Analysis and Design, 42 (2006) 1314-1323.
[26] Q.H. Qin, X.Q. He, Special elliptic hole elements of Trefftz FEM in stress concentration analysis, Journal of Mechanics and MEMS, 1 (2009) 335-348.
[27] Z.J. Fu, Q.H. Qin, W. Chen, Hybrid-Trefftz finite element method for heat conduction in nonlinear functionally graded materials, Engineering Computations, 28 (2011) 578-599.
[28] J. Jirousek, Q.H. Qin, Application of hybrid-Trefftz element approach to transient heat conduction analysis, Computers & Structures, 58 (1996) 195-201.
[29] Q.H. Qin, Hybrid Trefftz finite-element approach for plate bending on an elastic foundation, Applied Mathematical Modelling, 18 (1994) 334-339.
[30] Q.H. Qin, Postbuckling analysis of thin plates by a hybrid Trefftz finite element method, Computer Methods in Applied Mechanics and Engineering, 128 (1995) 123-136.
[31] Q.H. Qin, Transient plate bending analysis by hybrid Trefftz element approach, Communications in Numerical Methods in Engineering, 12 (1996) 609-616.
[32] Q.H. Qin, Postbuckling analysis of thin plates on an elastic foundation by HT FE approach, Applied Mathematical Modelling, 21 (1997) 547-556.
[33] F. Jin, Q.H. Qin, A variational principle and hybrid Trefftz finite element for the analysis of Reissner plates, Computers & structures, 56 (1995) 697-701.
[34] J. Jirousek, A. Wroblewski, Q.H. Qin, X. He, A family of quadrilateral hybrid-Trefftz p-elements for thick plate analysis, Computer Methods in Applied Mechanics and Engineering, 127 (1995) 315-344.
[35] Q.H. Qin, Hybrid-Trefftz finite element method for Reissner plates on an elastic foundation, Computer Methods in Applied Mechanics and Engineering, 122 (1995) 379-392.
[36] Q.H. Qin, Nonlinear analysis of thick plates by HT FE approach, Computers & structures, 61 (1996) 271-281.
[37] Q.H. Qin, S. Diao, Nonlinear analysis of thick plates on an elastic foundation by HT FE with p-extension capabilities, International Journal of Solids and Structures, 33 (1996) 4583-4604.
[38] C.Y. Lee, Q.H. Qin, H. Wang, Trefftz functions and application to 3D elasticity, Computer Assisted Mechanics and Engineering Sciences, 15 (2008) 251-263.
[39] Q.H. Qin, Variational formulations for TFEM of piezoelectricity, International Journal of Solids and Structures, 40 (2003) 6335-6346.
[40] Q.H. Qin, Solving anti-plane problems of piezoelectric materials by the Trefftz finite element approach, Computational Mechanics, 31 (2003) 461-468.
[41] Q.H. Qin, Mode III fracture analysis of piezoelectric materials by Trefftz BEM, Structural Engineering and Mechanics, 20 (2005) 225-240.
[42] Q.H. Qin, K.Y. Wang, Application of hybrid-Trefftz finite element method fractional contact problems, Computer Assisted Mechanics and Engineering Sciences, 15 (2008) 319-336.
[43] K. Wang, Q.H. Qin, Y. Kang, J. Wang, C. Qu, A direct constraint‐Trefftz FEM for analysing elastic contact problems, International journal for numerical methods in engineering, 63 (2005) 1694-1718.
[44] H. Wang, Q.H. Qin, Fundamental-solution-based finite element model for plane orthotropic elastic bodies, European Journal of Mechanics-A/Solids, 29 (2010) 801-809.
[45] H. Wang, Q.H. Qin, Fundamental solution-based hybrid finite element analysis for non-linear minimal surface problems, Recent Developments in Boundary Element Methods: A Volume to Honour Professor John T. Katsikadelis, (2010) 309.
[46] H. Wang, Q.H. Qin, Numerical implementation of local effects due to two-dimensional discontinuous loads using special elements based on boundary integrals, Engineering Analysis with Boundary Elements, 36 (2012) 1733-1745.
[47] H. Wang, Q.H. Qin, Special fiber elements for thermal analysis of fiber-reinforced composites, Engineering Computations, 28 (2011) 1079-1097.
[48] C. Cao, Q.H. Qin, A. Yu, Hybrid fundamental-solution-based FEM for piezoelectric materials, Computational Mechanics, 50 (2012) 397-412.
[49] C. Cao, A. Yu, Q.H. Qin, A new hybrid finite element approach for plane piezoelectricity with defects, Acta Mechanica, 224 (2013) 41-61.

[50] H. Wang, Q.H. Qin, Fracture analysis in plane piezoelectric media using hybrid finite element model, in: The 13th International Conference on Fracture, 2013.
[51] C. Cao, Q.H. Qin, A. Yu, A new hybrid finite element approach for three-dimensional elastic problems, Archives of Mechanics, 64 (2012) 261–292.
[52] H. Wang, L. Cao, Q.H. Qin, Hybrid Graded Element Model for Nonlinear Functionally Graded Materials, Mechanics of Advanced Materials and Structures, 19 (2012) 590-602.
[53] H. Wang, Q.H. Qin, Boundary Integral Based Graded Element For Elastic Analysis of 2D Functionally Graded Plates, European Journal of Mechanics-A/Solids, 33 (2012) 12-23.
[54] H. Wang, Q.H. Qin, FE approach with Green's function as internal trial function for simulating bioheat transfer in the human eye, Archives of Mechanics, 62 (2010) 493-510.
[55] H. Wang, Q.H. Qin, Computational bioheat modeling in human eye with local blood perfusion effect, in: Human Eye Imaging and Modeling, CRC Press, 2012, pp. 311-328.
[56] H. Wang, Q.H. Qin, A fundamental solution based FE model for thermal analysis of nanocomposites, Boundary elements and other mesh Reduction methods XXXIII', 33rd International Conference on Boundary Elements and other Mesh Reduction Methods, ed. CA Brebbia and V. Popov, WIT Press, UK, (2011) 191-202.
[57] H. Wang, Q.H. Qin, A new special element for stress concentration analysis of a plate with elliptical holes, Acta Mechanica, 223 (2012) 1323-1340.
[58] H. Wang, Q.H. Qin, Implementation of fundamental-solution based hybrid finite element model for elastic circular inclusions, in: The Asia-Pacific Congress for Computational Mechanics, 2013.
[59] H. Wang, Q.H. Qin, W.-A. Yao, Improving accuracy of opening-mode stress intensity factor in two-dimensional media using fundamental solution based finite element model, Australian Journal of Mechanical Engineering, 10 (2012) 41-52.
[60] Z.-W. Zhang, H. Wang, Q.H. Qin, Transient Bioheat Simulation of the Laser-Tissue Interaction in Human Skin Using Hybrid Finite Element Formulation, MCB: Molecular & Cellular Biomechanics, 9 (2012) 31-54.
[61] H. Wang, Q.H. Qin, A fundamental solution-based finite element model for analyzing multi-layer skin burn injury, Journal of Mechanics in Medicine and Biology, 12 (2012) 1250027.
[62] C.B. Morrey, Multiple integrals in the calculus of variations, Springer Science & Business Media, 2009.
[63] J. Katsikadelis, M. Nerantzaki, G. Tsiatas, The analog equation method for large deflection analysis of membranes. A boundary-only solution, Computational Mechanics, 27 (2001) 513-523.
[64] H. Wang, Q.H. Qin, Y. Kang, A new meshless method for steady-state heat conduction problems in anisotropic and inhomogeneous media, Archive of Applied Mechanics, 74 (2005) 563-579.
[65] H. Wang, Q.H. Qin, Y. Kang, The method of fundamental solutions with radial basis functions approximation for thermoelastic analysis, Journal of Dalian University of Technology, 46, S1 (2006) 46-51.
[66] R. Schaback, Error estimates and condition numbers for radial basis function interpolation, Advances in Computational Mathematics, 3 (1995) 251-264.
[67] C. Chao, M. Shen, On bonded circular inclusions in plane thermoelasticity, Journal of applied mechanics, 64 (1997) 1000-1004.
[68] V. Kupradze, M. Aleksidze, The method of functional equations for the approximate solution of certain boundary value problems, USSR Computational Mathematics and Mathematical Physics, 4 (1964) 82-126.
[69] P. Mitic, Y.F. Rashed, Convergence and stability of the method of meshless fundamental solutions using an array of randomly distributed sources, Engineering Analysis with Boundary Elements, 28 (2004) 143-153.
[70] H. Wang, Q.H. Qin, Y. Kang, A meshless model for transient heat conduction in functionally graded materials, Computational mechanics, 38 (2006) 51-60.
[71] H. Wang, Q.H. Qin, Some problems with the method of fundamental solution using radial basis functions, Acta Mechanica Solida Sinica, 20 (2007) 21-29.
[72] D. Young, S. Jane, C. Fan, K. Murugesan, C. Tsai, The method of fundamental solutions for 2D and 3D Stokes problems, Journal of Computational Physics, 211 (2006) 1-8.
[73] L. Marin, D. Lesnic, The method of fundamental solutions for nonlinear functionally graded materials, International journal of solids and structures, 44 (2007) 6878-6890.
[74] J. Berger, P. Martin, V. Mantič, L. Gray, Fundamental solutions for steady-state heat transfer in an exponentially graded anisotropic material, Zeitschrift für angewandte Mathematik und Physik ZAMP, 56 (2005) 293-303.
[75] L. Gray, T. Kaplan, J. Richardson, G.H. Paulino, Green's functions and boundary integral analysis for exponentially graded materials: heat conduction, Journal Of Applied Mechanics, 70 (2003) 543-549.
[76] J. Liu, L.X. Xu, Boundary information based diagnostics on the thermal states of biological bodies, International Journal of Heat and Mass Transfer, 43 (2000) 2827-2839.
[77] L. Cao, Q.H. Qin, N. Zhao, An RBF–MFS model for analysing thermal behaviour of skin tissues, International Journal of Heat and Mass Transfer, 53 (2010) 1298-1307.
[78] K.S. Frahm, O.K. Andersen, L. Arendt-Nielsen, C.D. Mørch, Spatial temperature distribution in human hairy and glabrous skin after infrared CO2 laser radiation, Biomedical engineering online, 9 (2010) 69.
[79] Z.P. Ren, J. Liu, C.C. Wang, P.X. Jiang, Boundary element method (BEM) for solving normal or inverse bio-heat transfer problem of biological bodies with complex shape, Journal of Thermal Science, 4 (1995) 117-124.
[80] M. Golberg, C. Chen, H. Bowman, H. Power, Some comments on the use of radial basis functions in the dual reciprocity method, Computational mechanics, 21 (1998) 141-148.
[81] A. Muleshkov, M. Golberg, C. Chen, Particular solutions of Helmholtz-type operators using higher order polyhrmonic splines, Computational mechanics, 23 (1999) 411-419.
[82] K. Balakrishnan, P. Ramachandran, The method of fundamental solutions for linear diffusion-reaction equations, Mathematical and Computer Modelling, 31 (2000) 221-237.